THESIS FOR THE DEGREE OF MASTER OF SCIENCE IN CHEMICAL ENGINEERING

Reprocessing and Characterization of Polybenzimidazole for High-Temperature Polymer Electrolyte Membrane Fuel Cells

BY DOUGLAS BJÖRKENGREN

LUND UNIVERSITY

Supervisors: David Aili, Patric Jannasch, Lars Nilausen Cleemann
Co-supervisor: Sinu C. Rajappan
Examiner: Baozhong Zhang

Centre for Analysis and Synthesis
Department of Chemistry
Lund University

August 2023

Abstract

A reprocessing method of poly(2,2'-(*m*-phenylene)-5,5'-bibenzimidazole) (PBI) membranes recovered from the production line of High-Temperature Polymer Electrolyte Membrane Fuel Cells (HT-PEMFC) at Blue World Technologies (BWT) has been developed in order to reduce material loss in the production. Redissolution of scrap PBI membranes in poly(phosphoric acid) (PPA) and phosphoric acid (PA) was successful and the subsequent washing procedure produced PBI that could be redissolved in *N,N*-dimethyl acetamide (DMAc) and suitable for solution casting of new membranes. The reprocessed PBI and the membranes cast from it were characterized with respect to molecular weight, structural purity, acid doping behavior, thermal stability, mechanical strength, proton conductivity and fuel cell performance using pristine PBI membranes as the reference point. A reduction of the molecular weight was observed after the redissolution, which was speculated to be caused by hydrolysis of weak amide bonds due to structural defects in the polymer backbone. After doping in 85 wt.% PA, the tensile properties and the ex-situ proton conductivity were slightly decreased in comparison to the pristine reference material which could reasonably be explained by deviations in the membrane thickness and doping level. No apparent difference in properties depending on which solvent was used in the redissolution was observed. Fuel cell testing indicated similar performance between reprocessed and pristine PBI membranes, thus demonstrating the viability of the attempted recycling method.

Acknowledgements

This master thesis project was conducted during the spring semester of 2023 in cooperation with Blue World Technologies (BWT) in Kvistgård and the Department of Energy Conversion and Storage at the Technical University of Denmark (DTU). It was performed as a part of the exchange program between the Faculty of Engineering at Lund University and DTU.

I would like to thank all involved parts at BWT for providing me the opportunity to perform this project. I am thankful to all the employees at the BWT facilities in Kvistgård who have helped me during this time, especially Lars Nilausen Cleemann for his supervision and guidance.

Furthermore, I would like to show my gratitude to David Aili and Sinu C. Rajappan at the Department of Energy Conversion and Storage at the Technical University of Denmark for all the counselling, assistance and inspiration that they have provided me with during the project.

I am also obliged to Patric Jannasch and Baozhong Zhang at the Department of Chemistry, Faculty of Engineering, Lund University who led me into to this exciting area of chemistry.

To my family, thank you for your everlasting support and encouragement. I am especially grateful to my sister – Gabriella – who has always served as a great inspiration for me in all of my pursuits.

Table of contents

1. Introduction

Fuel cells are electrochemical devices that convert the chemical energy of a fuel into electricity through electrochemical reactions. In recent years, it has come of great interest for powering automotive and maritime vehicles, industrial and residential buildings as well as for back-up power systems as a way to combat the release of greenhouse gases that are emitted from the use of combustion engines running on fossil fuels [1]. Fuel cells can be classified by the type of electrolyte that it utilizes, one such is the Polymer Electrolyte Membrane Fuel Cell (PEMFC) that commonly incorporates so called Polymer Electrolyte Membranes (PEM). The PEM is part of the Membrane Electrode Assembly (MEA), which is the component in the fuel cell where the electrochemical reactions occur. The purpose of the PEM in the fuel cell is to act as an electrolyte for which protons are able to pass through, provide a barrier to separate oxygen and hydrogen gas and also to act as a support for the electrode catalysts and electronic insulator [1].

To increase the viability of the PEMFC technology and realize its potential to replace conventional fossil fuel combustion engines as a means for power generation, there are areas that need to be improved to increase the performance of the fuel cell systems as well as reducing the over-all cost of producing them. Proton conductivity, stability under thermally, mechanically and chemically harsh conditions and an acceptable durability over extended operation times [2] are essential aspects of the technology that are currently being addressed through fundamental and applied research in order to optimize performance. Additionally, it is of great importance that the materials that are used to manufacture the fuel cells are readily available to produce, easy to work with and possible to recycle in an environmentally friendly manner [2].

PEMFC technology can be divided into two different areas based on the operational temperature of the system. Low Temperature PEMFCs (LT-PEMFC) are considered to be systems that are designed to typically operate at 80 °C. High Temperature PEMFCs (HT-PEMFC) instead operate at a temperature range of 100-200 °C. In the last two decades, the HT-PEMFC technology has received an increasing amount of attention as it has been established that it offers advantages over the low temperature counterpart that leads to increased efficiency of the fuel cell system as well as unique benefits in terms of the overall system design [3]. The possibility to use polybenzimidazole (PBI) doped with phosphoric acid (PA) as a proton conducting electrolyte was first discovered in the groundbreaking research made at the Case Western Reserve University by Wainright et al. [4], and has since emerged to become the current state-of-the-art PEM material for HT-PEMFC technology.

1.1 Project description

Blue World Technologies (BWT) is a Danish company founded in 2018 and based in Aalborg, that manufactures and develops HT-PEMFC systems for a range of industries but is primarily targeted towards stationary power system applications and the maritime sector [5]. In 2020 BWT acquired Danish Power Systems (DPS), a research and development company located in Kvistgård - north of Copenhagen - with extensive experience and knowledge of HT-PEM-technology. At the facilities in Kvistgård, BWT is currently conducting research and development of MEAs including the commercialized Dapozol® MEA that was originally developed by DPS. Additionally, the synthesis and quality control of the PBI that is used to produce the PEMs is performed in Kvistgård. Further processing of the membranes is carried out in a newly built factory in Aalborg and includes shaping of the membranes to fit the required dimensions of the MEAs, a step that leads to the unavoidable loss of membrane material. To reduce the associated economic and environmental costs, BWT would like to find a way to recover the PBI scrap so that it can be re-fed into their membrane production line.

1.2 Aim and scope

The purpose of this master thesis project is to investigate the possibility for recycling of scrap PBI membranes from the production line of BWT. The goal is to find a reprocessing method that yields PBI of sufficient quality so that it is possible to use it to cast new membranes that can be used in the MEA production. The evaluation of the reprocessing method will be based on qualitative observations as well as quantitative measurements through characterization methods that are commonly used to analyze the physicochemical properties of PEM materials. Additionally, the fuel cell performance of the reprocessed PBI membranes will be investigated. The results will be benchmarked against pristine PBI membranes to compare the quality of the material before and after reprocessing.

2. Background

2.1 PEMFC description

The PEMFC was first designed by General Electric in the 1960's as part of the effort to develop power systems for space applications [6]. A PEMFC operates on the same principles as a battery, with the difference being that the PEMFC can keep supplying power as long as a chemical fuel is fed that can be converted into electrical energy. Most commonly, hydrogen gas is the choice of fuel as it offers several advantages over liquid fuels such as methanol and ethanol in terms of reaction kinetics and prevention of fuel cross-over between the two electrodes [6]. However, fuel cell systems that implement reformation of liquid fuels into hydrogen gas that is then fed to the MEA has in the last decade found major interest. For an example, BWT has opted to utilize methanol reformed hydrogen gas which allows for easy distribution and storage in comparison with gaseous fuels that would require pressurization to be effectively transported [5]. This approach combines the benefits of using an easily transported liquid with the improved efficiency of hydrogen gas fuel. A net-zero carbon emissions operation with no SO_x, NO_x or other particle emissions can be obtained if renewable methanol is used to power the fuel cell system [5].

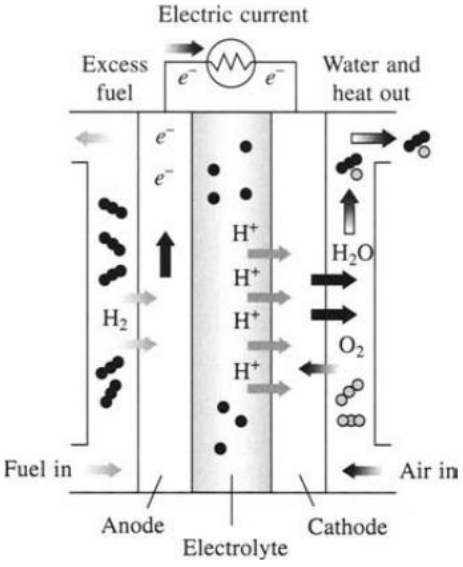

Figure 2.1: A schematic picture of a PEM fuel cell [6].

The heart of the PEMFC is the MEA which is where the electrochemical reactions occur. The basic design of the MEA is displayed in Figure 2.1. It consists of two carbon supported gas diffusion electrodes (GDE) – anode and cathode – that are separated by the ionically conducting PEM. The PEM is sandwiched between the two electrodes that are impregnated with an ink containing metal particles (commonly platinum (Pt) and cobalt (Co)) that catalyzes the electrochemical reactions. The side of the electrodes that are not facing the PEM are usually coated with a hydrophobic substance such as Teflon, to direct the fuel gas flow to the catalysts. When the fuel reaches the anode it is oxidized into protons and electrons via the hydrogen oxidation reaction (HOR) (Eq. 2.1). The electrons are conducted along an external circuit

creating an electric current. Meanwhile the protons are conducted through the electrolyte to the cathode that is being supplied with oxygen. The protons and the oxygen react to form water through the oxygen reduction reaction (ORR) (Eq. 2.2).

Eq. 2.1 $$H_2 \rightarrow 2\,H^+ + 2\,e^-$$

Eq. 2.2 $$O_2 + 4\,H^+ + 4\,e^- \rightarrow 2\,H_2O$$

The theoretical cell voltage of a single cell under standard conditions is 1.23 V but typically, the practical open circuit voltage (OCV) that is obtained is just below 0.9 V. To obtain a higher cell voltage, fuel cell systems are designed so that multiple cells are connected in series, which is commonly referred to as a fuel cell stack. The size of the fuel cell stack can be varied depending on the required power output for a certain application [6]. Naturally, the power output of the fuel cell becomes directly related to the proton conductivity of the PEM and it is therefore a highly important property of the membrane. In addition, the PEM needs to be electronically insulating to prevent short circuiting, have a high mechanical strength and resistance to degradation and also be stable under harsh chemical conditions [6]. These properties also need to be retained during extended time periods of operation and the durability of PEMFC systems is a key performance factor.

2.2 Advantages of High-Temperature operation

The current state of the art technology for LT-PEMFC uses PEMs based on polyperfluorosulfonic acid (PFSA) as it offers a high proton conductivity while also providing high chemical and thermal resistance due to the perfluorinated polymer backbone. Proton conductivity in PFSA membranes is only obtained under highly humidified conditions as it is the presence of water in the membrane that makes it ionically conducting [7]. By interaction with the sulfonic acid side chain groups in the PFSA, the water forms hydrated domains in the membrane which acts as a medium through which the protons are able to pass through. Clearly, the requirement of humid conditions makes operation at elevated temperatures difficult as the vapor pressure of water increases with the temperature. To avoid evaporation of water, and thus loss of proton conductivity, operation above the boiling point of water would require the system to be pressurized which increases the complexity of the fuel cell design [7].

While LT-PEMFCs has proven to be a successful option in many cases, it is hindered by a few issues that are detrimental for the fuel cell technology to be able to compete with combustion engines in terms of efficiency and economic viability. Four aspects have been identified as the main issues of LT-PEMFCs which include [3]: (1) low tolerance for fuel impurities due to catalyst poisoning, (2) need for water management systems to keep the PEM humidified, (3) need for cooling systems to control the temperature of the fuel cell system and (4) poor electrode kinetics. To combat these issues there has been an incentive to develop the HT-PEMFC

technology since it has been established that the detrimental effects by the presented issues can be minimized or resolved simply by increasing the operating temperature [7].

HT-PEMFCs are designed to operate at higher temperatures than the low temperature counterpart in order to improve the efficiency of the fuel cell system. The increased temperature dramatically increases the tolerance for carbon monoxide and other impurities that can be present in the fuel [3]. This allows fuels with a lower purity to be used and thus the complexity of the purification process of the methanol-reformed hydrogen gas can be simplified or even eliminated. Hence, the production costs, size and start-up time of the fuel cell system can be greatly reduced. Since the PEM in HT-PEMFCs is not reliant on the presence of water to attain a high proton conductivity, water management systems can be greatly simplified. Because the typical operating temperature is above the boiling point of water, only the vapor phase is present in the system which eliminates issues related to condensation, such as flooding of gas diffusion channels and localized dehydration due to water drag [3]. The complexity of the cooling system can also be minimized due to the increased temperature gradient between the fuel cell stack and the surrounding environment which facilitates heat removal. Additionally, the higher temperature of the produced heat increases its value and it can thus be used in other processes that occur in the fuel cell system, e.g. pressurizing inlet gas, mechanical work, evaporation of water and for heating of the reformer [3]. Finally, the temperature increase improves the reaction kinetics for both the cathode and the anode electrodes in the MEA, which is especially important for the ORR reaction at the cathode which is rate limiting. However, it must be pointed out that the expected improvement of the kinetics is not seen in the PBI/PA system due to the strong adsorption of PA to the surface of the Pt catalyst particles [3]. If pure hydrogen gas is used, the overall result is actually that the kinetics are worse for the HT-PEMFC in comparison to the LT-PEMFC.

2.3 Polymer recycling

The production of materials based on synthetic polymers has grown immensely since they were first discovered in the early 1920's. Today, over 380 million tons of plastics are produced annually with up to 50% consisting of single-use plastics that are used only briefly before being discarded [8]. For a long time the main way of handling plastic waste has been to either bury it in the ground as landfill or incinerate it for energy production. However, the increasing demand for reduction of greenhouse gas emissions has forced the polymer industry to strive to become more sustainable and environmentally friendly. A lot of research has been put into finding new types of polymers that can be produced from bio-based resources and that are ideally also bio-degradable [8]. Nevertheless, a large portion of the plastics that are used today are currently not able to be replaced by alternative polymers. Therefore, it has instead been attempted to develop methods for recycling of plastics to reduce the volume of new production [8].

There are mainly two approaches for recycling of polymer waste: mechanical- and chemical recycling. The first option involves grinding of the waste which is then reprocessed and compounded into new polymer material [9]. Chemical recycling is used to return the polymer waste to hydrocarbon components or monomers. These may be used to produce new polymer

materials but they can also be used to reproduce the pure polymer [9]. Mechanical recycling is the more widely employed option due to its reliability and low cost. Typically, CO_2 emissions can be reduced by more than 80% by applying mechanical recycling of plastic waste products as opposed to new production [10]. It must be considered that repeated recycling of polymers can have an impact on the properties of the material due to a decrease in the molecular weight caused by the recycling processing. As such, many polymers can only withstand a certain amount of recycling cycles before there is a significant loss of properties [8]. Another issue that is presented is the need for separation of different polymer species. A lot of polymers are incompatible for mixing due to low adhesion and phase separation which causes poor mechanical properties [9] and conventional industries often require polymer purities of at least 96% [11]. Therefore, it is required to separate the waste based on their chemical composition before they are recycled. In recent years, there has been a lot of progress in the development of plastic separation methods. For an example, a research project lead by Aarhus University developed a camera technology based on infra-red spectroscopy that was able to distinguish 12 different common consumer plastics [11].

Overall, the global recycling rate of plastics is relatively small. In 2018, barely 9% of all plastics were recycled [12], however recycling rates for certain polymers is remarkably higher than for others. Naturally, the research on polymer recycling so far has been focused on the polymers that are used to produce the common commodity plastics that make up the large majority of polymeric material production. By far the most widely recycled polymer material globally is poly(ethylene terephthalate) (PET), with some parts of the world reaching recycling rates higher than 50% [9]. PET is mostly employed in plastic bottle and container production. Aside from reproduction of new bottles, a common product of the recycling process is found in clothes and textiles. High-density polyethylene (HDPE) has also been successfully recycled although not to the same extent as PET. In the US it is estimated that around 30% [12] of the HDPE used in bottle manufacturing is recycled. Similarly to PET, the recycled HDPE polymer is mostly used to produce the same type of products as before recycling. The third commodity polymer that sees frequent recycling is polypropylene (PP). Due to difficulties in retaining the polymers original appearance and properties, the products of recycled PP usually differ from its original products [8]. Newly produced PP is regularly used in food packing and bottles but due to difficulties in removing smell in addition to its grey coloring, recycled PP is mostly used in alternative products such as speed bumps, automotive parts and in industrial applications. Recycling of engineering polymers is today highly limited and not much research is available on the topic. However, with growing demands on sustainability and reduction of greenhouse gas emissions it is possible that it will see increasing importance within relevant industries in the future.

3. Polybenzimidazole: Synthesis, properties and membrane casting

The structurally most simple PBI is AB-PBI which is obtained from the homopolymerization of 3,4-diaminobenzoic acid. AB-PBI displays excellent mechanical properties and chemical resistance and the use of a single monomer removes the issue of stoichiometric control which can be a limiting factor when attempting to achieve high molecular weight polymers [13]. However, the use of AB-PBI has been found to be problematic due to its low solubility in organic solvents which makes it difficult to process for use in fuel cell applications. The PBI that has been most developed towards commercial applications and is currently seen as the option of choice in fuel cell systems is poly(2,2'-(*m*-phenylene)-5,5'-bibenzimdiazole) abbreviated as *m*-PBI but commonly referred to as simply PBI. It differs from AB-PBI in that it contains a flexible *m*-phenylene linkage between the benzimidazole units, significantly increasing the polymers solubility in organic solvents [13]. Due to its good processing characteristics, it has found usage as fibers for temperature resistant fabrics and coatings [14]. The repeat units of *m*-PBI and AB-PBI can be seen in Figure 3.1.

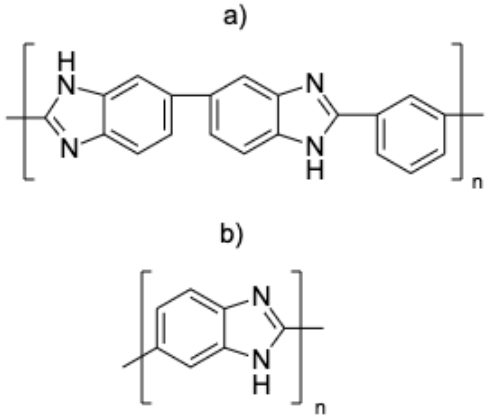

Figure 3.1: The repeat units of (a) m-PBI and (b) AB-PBI.

3.1 Synthesis

The first PBIs were discovered and successfully synthesized in the 1960's by Marvel and Vogel [15], and were spun into fibers that were used in firefighter's apparel, astronaut space suits and aircraft wall fabrics. The synthesis was carried out in a melt-condensation process with diamines and dicarboxylic acids as the monomers. An alternative polymerization process using poly(phosphoric acid) (PPA) to dissolve the monomers was discovered by Iwakura et. al [16] shortly after and has since become a common method for PBI preparation. In this approach, *m*-PBI is attained via the polycondensation reaction of isophathalic acid (IPA) and 3,3'-diaminobenzidine (DAB), which can be seen in Figure 3.2. It should be mentioned that the polymerization reaction is carried out in a highly acidic environment and thus the amine-groups in DAB is protonated into ammonium ions which have a relatively low reactivity. Therefore, the reaction requires high temperatures and long reaction times. A typical process is carried out by dissolution of 3-5 wt.% of solid monomers in PPA with the temperature being increased up to 170-230 °C over time periods ranging from a few hours to several days depending on the

required degree of polymerization [3]. The water that is formed from the condensation reaction is consumed by the hydrolytic splitting of PPA which contributes to the formation of products according to Le Chatelier's principle [13]. To achieve a high linear molecular weight it is of crucial importance to minimize side reactions - primarily chain branching and cross-linking – which is done by optimizing the polymerization temperature and reaction time [17]. Additionally, a high monomer purity and accurate stoichiometry is required based on Carother's equation [18]. Research has proven that the polycondensation reaction can be accelerated by using micro-wave assisted heating without lowering the molecular weight of the obtained polymers [19], [20]. The polymer is readily precipitated by pouring out the solution in water. It requires meticulous washing since any acid residues will hinder the dissolution of PBI in organic solvents.

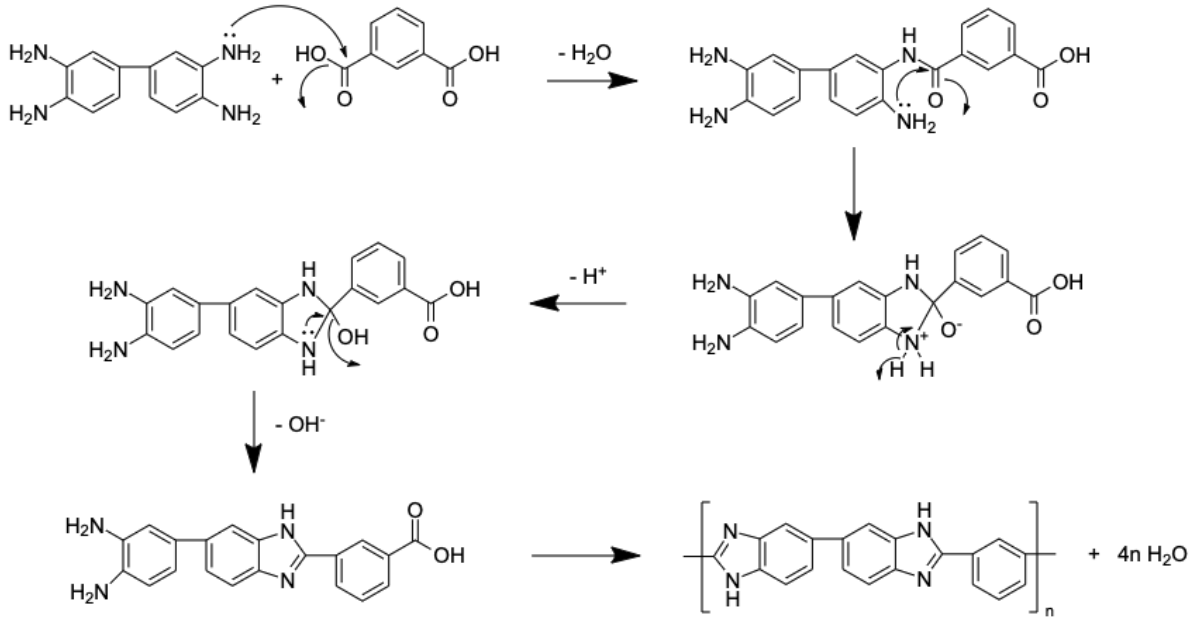

Figure 3.2: Reaction mechanism for the polycondensation reaction of IPA and DAB to form m-PBI.

A lot of PBI chemistries – especially those that include large aromatic side chain units - are not possible to synthesize using PPA as the polycondensation solvent due to poor solubility and susceptibility to side reactions in PPA. In this case it is possible to utilize a mix of MSA and phosphorous pentoxide - commonly referred to as Eaton's reagent – to dissolve the monomers [13]. In general, synthesis pathways utilizing Eaton's reagent usually display a shorter reaction time while also requiring lower reaction temperatures.

3.2 Properties

3.2.1 Thermal and mechanical properties

PBI is an engineering plastic that is characterized by excellent thermal and chemical resistance, which is attributed to the inclusion of the highly stable benzimidazole unit. It displays an

exceptionally high glass transition temperature of 425-435 °C [14] - the highest of any commercially available polymer - which is explained by the stiffness of the fully aromatic and heterocyclic polymer backbone as well as the strong intermolecular hydrogen bonding between the benzimidazole groups [21]. It is a thermoplastic polymer that is fully amorphous and therefore it has no melting temperature. The thermal decomposition temperature of PBI when exposed to oxygen atmospheres for longer durations is around 350 °C [22]. Although the polymer is able to withstand loss of mechanical properties for short time periods at temperatures above the decomposition temperature [23]. Because of these properties it has found usage in several applications that require high thermal and chemical stability such as material for firefighter's apparel and astronaut suits.

When doped with PA the mechanical properties of PBI is significantly changed due to the plasticizing effect that is associated with the acid uptake which causes swelling and consequently separation of the polymer chains [1]. When there is a large excess of acid present in the PBI matrix the loss of mechanical properties can become problematic. To circumvent this issue it has been attempted to use high molecular weight PBI [24] as well cross-linking the polymer chains to improve the mechanical strength [22]. Another proposition has been to integrate different chemical units into the polymer backbone. For an example, Li et al. [25] found that the yield strength could be improved from 11.6 MPa for pure PBI to 19.8 MPa when -C(CF_3)- bridging groups were introduced into the structure, which was believed to be because of reduced swelling and thus less separation of the polymer chains post-doping.

3.2.2 Solubility

PBI is soluble in strong protic acids such as sulfuric acid, hydrochloric acid and poly(phosphoric acid) (PPA) [19]. The solubility in organic solvents is generally poor and there are only a few available options that consist of polar aprotic solvents. PBI displays a high solubility in *N,N*-dimethyl acetamide (DMAc), which is governed by the development of hydrogen bonding interactions between the polymer and the solvent [26], but also the formation of charge transfer complexes between the benzene rings in PBI and the DMAc molecules [27]. It is commonly used to dissolve PBI as it gives polymer solutions with appropriate viscosities for spinning of fibers and film casting [28]. Other common organic solvents that can be used include dimethyl sulfoxide (DMSO) and *N,N*-dimethyl formamide (DMF). The use of ionic liquids, e.g. 1-butyl-3-methylimidazolium, as a solvent has recently been investigated as it would allow for a more environmentally friendly option in comparison to the earlier mentioned solvents [29].

It should be noted that the high solubility seen in some organic solvents is unique to m-PBI and is attributed to the meta-phenylene linkage in the structure [13]. Other common PBIs such as *p*-PBI and AB-PBI are only soluble in methane sulfonic acid (MSA) among the organic solvents [19]. One of the main goals of the research based around finding new PBI chemistries is to improve the organo-solubility. This has been done by modifications of the polymer backbones and grafting of side chains to reduce the intermolecular forces between the polymer chains which increases the solubility in organic solvents. Some examples of modifications to the PBI

structure include additions of ether-, sulfone- and hexafluoroisopropylidene groups, which have all shown to drastically improve the organosolubility [30], [31].

3.2.3 Acid doping and proton conductivity

PBI in itself is non-conductive and the amphoteric nature of the benzimidazole group imply that it responds to pH changes by protonation/deprotonation [13]. When exposed to protic acids the benzimidazole functional group is protonated, forming polybenzimidazoliums with a pK_{aH} of 5.6 [32]. This functionalization increases the polarity of the backbone which allows for further uptake of excess acid, which results in a proton conducting material that is suitable for use as the electrolyte in PEMFCs. As the benzimidazole functionality allows for the formation of hydrogen bonding it makes PBI highly hydrophilic with an equilibrium moisture content of 15-19% [23].

PA is commonly used as the dopant of choice since it shows a high thermal stability and proton conductivity up to 210 °C, which makes it suitable for HT-PEM applications. Other acids that have been proposed include e.g. sulfuric acid, hydrochloric acid and nitric acid [33]. It has been observed that a high proton conductivity can only be achieved when doping with amphoteric acids, i.e. acids that can act both as proton donors and acceptors. Sulfuric acid has been proven to produce an even higher proton conductivity than what may be achieved when using PA [34], however, its relatively high vapor pressure has shown to be an obstacle since it leads to higher rates of acid evaporation. The doping process is performed by submerging the PBI membranes in PA for an extended time period. The ambient temperature and the concentration of the PA has an influence on the amount of acid that the membrane takes up. The PA uptake is often normalized as the acid doping level (ADL), defined as the number of PA molecules per repeat unit of PBI, see 4.3. Phosphoric acid uptake. The maximum degree of protonation for *m*-PBI is reached at an ADL of 2, i.e. two dihydrogenphosphate anions that are associated to each repeat unit [35]. At this ADL the proton conductivity is low (10^{-6} S cm^{-1}), which is insufficient in fuel cell applications. The conductivity rapidly increases as the PA content is increased so that it is present in an excess as 'free acid' [35]. In recent years the conductivity has been improved from roughly 0.05 to 0.10 S cm^{-1}, which has been achieved by the successful synthesis of high molecular weight PBI that can obtain higher doping levels (10-12) and still sufficiently retain its mechanical strength [32].

The unique chemical nature of the proton provides two fundamental conduction mechanisms. The first one is based on a vehicular mechanism where the protons are transported throughout a medium by associating to a carrier- molecule or ion to form a protonated species, e.g. OH^{-}, H_3O^+ or $H_4PO_4^+$. This mechanism is predominating for the proton conduction in PEMs based on poly(perfluorosulfonic acid) as the terminal sulfonic acid groups create continuous hydrated domains that protons can pass through by associating to water molecules [3]. The other mechanism is based on the formation of dynamic hydrogen bonding networks that allows protons to readily create and break hydrogen bonds [37] – the so called Grotthuss mechanism. Recent research indicates that the Grotthuss mechanism is strongly dependent on the water content of the system and it has been suggested that it is only the dominating conduction mode

within a narrow temperature and composition range [13]. Outside of this range the contribution of the vehicular mechanism becomes increasingly more substantial, which results in redistribution of the doping acid during fuel cell operation. Particularly at high current loads, when the rate of migration exceeds the rate of back diffusion [36].

3.3 Membrane casting

The choice of method for preparation and casting of PBI membranes has proven to have an impact on the properties of the membranes [19]. A few different techniques have been reported in the literature that all offer different advantages.

3.3.1 Solution casting

The most common way of casting PBI membranes is by organic solvent evaporation. It utilizes the solubility of PBI in DMAc to create a polymer solution from which membranes can be casted. For PBI within the inherent viscosity range of 0.6-1.5 dL g^{-1}, a polymer solution with 2-10 wt.% of PBI in DMAc is suitable for membrane casting purposes. At higher concentrations the viscosity of the solution becomes too high to effectively cast membranes and the same issue can be seen in PBI with inherent viscosities above 1.5 dL g^{-1}. Additionally, problems with in-solution agglomeration may occur at higher polymer concentrations due to considerable hydrogen bonding interactions between the polymer chains [26]. To prevent this, lithium chloride (LiCl) may be added in small amounts to stabilize the solution. The stabilizing effect is believed to be explained by the disruption of hydrogen bonding between polymer chains caused by the coordination of the Li^+ cation to the benzimidazole groups [37].

Before the casting process is begun it is often beneficial to filter the polymer solution to remove any particles that may cause defects in the membranes. The membrane casting is commonly done by casting the polymer solution onto a substrate and then gradually heating it over an extended time period to promote a slow evaporation of the DMAc. This procedure is suitable for small-scale production for laboratory and research purposes, however, it is considerably time-consuming and inefficient when a high throughput of membranes is required. Steenberg et al. [38] employed roll-to-roll coating and determined that the manufacturing speed could be improved by a factor of 100 without any loss in properties compared to traditionally cast membranes.

3.3.2 The sol-gel method

In the sol-gel method the solubility of PBI in PPA is utilized to carry out both the polymerization and the acid doping in one step. After the polymerization reaction has been terminated, the crude solution is tape casted and exposed to an environment with carefully controlled temperature and humidity. The hygroscopic PPA absorbs moisture which induces hydrolysis into PA. The solubility of PBI in PA is relatively poor as opposed to PPA which gives rise to a sol-gel transition and membranes that can contain up to 40 PA molecules per polymer repeat unit [39]. It has been found that membranes prepared by this method obtains greater mechanical

strength and higher proton conductivity than membranes prepared by other methods at similar acid contents, which is likely explained by a difference in morphological features as compared to membranes that are solution cast from organic solvents [39]. Additionally, it also eliminates the associated environmental and safety issues as well as the costs that come with using organic solvents. There is currently ongoing research to investigate how to improve long-term durability of membranes cast from the sol-gel method.

3.3.3 The direct method

Alternatively, membranes may be cast from a method developed by CRWU [40]. In this method the casting and the doping is performed simultaneously by grinding the PBI into a fine powder which is dissolved in trifluoroacetic acid. It is thereafter mixed with PA to form a homogenous solution which is readily cast into membranes. It has been reported that the direct method produces PBI membranes with a greater proton conductivity than membranes that are solution cast from DMAc. The increased conductivity was suggested to be caused by an increase in the degree of crystallinity that creates proton conducting pathways through the membrane cross section by forcing the PA into amorphous regions [40]. Nevertheless, the increased crystallinity makes the membranes softer and more rubbery which lowers the mechanical strength. Therefore, high molecular weight PBI is required to provide membranes with sufficient mechanical properties.

3.3.4 Description of the membrane production process at BWT

A general description of the production process of PBI membranes at BWT is displayed in the process flow chart seen in Figure 3.3. Along the entire production line there is a continuous quality control of the PBI and the membranes casted from it which includes molecular weight measurements, evaluation of the casting solution properties and determination of the acid doping level, etc. These steps are however not included in the presented flow chart.

The production begins with the synthesis of PBI which is carried out by an optimized polycondensation reaction of the monomers DAB and IPA using PPA as the solvent (see Figure 3.2) - in order to obtain high molecular weights which is required for the production of mechanically strong membranes. The resulting PBI is put through a rigorous washing procedure to remove all of the absorbed acid which is required to make the polymer dissolvable in DMAc. Before the PBI can be dissolved it is thoroughly dried to prevent hydrolysis of the solvent. After dissolution in DMAc, the casting of the membranes is performed by a roll-to-roll coating process onto substrates to ensure a constant membrane thickness and a high throughput. The casted membranes are thereafter doped in 85 wt.% PA at room temperature to attain ADLs in the range of 10-12. Finally, the membranes are processed for use in the MEA production which includes calendering to remove excess acid and cutting of the membranes to fit the required dimensions for the MEA. It is in this step that the main loss of PBI from the production line occur due to the unavoidable loss of membrane material in the cutting procedure. Additionally, there are losses along the production line of PBI material that has not passed the quality control

– mainly due to failure in attaining the correct doping level – however, this is a relatively small contribution overall.

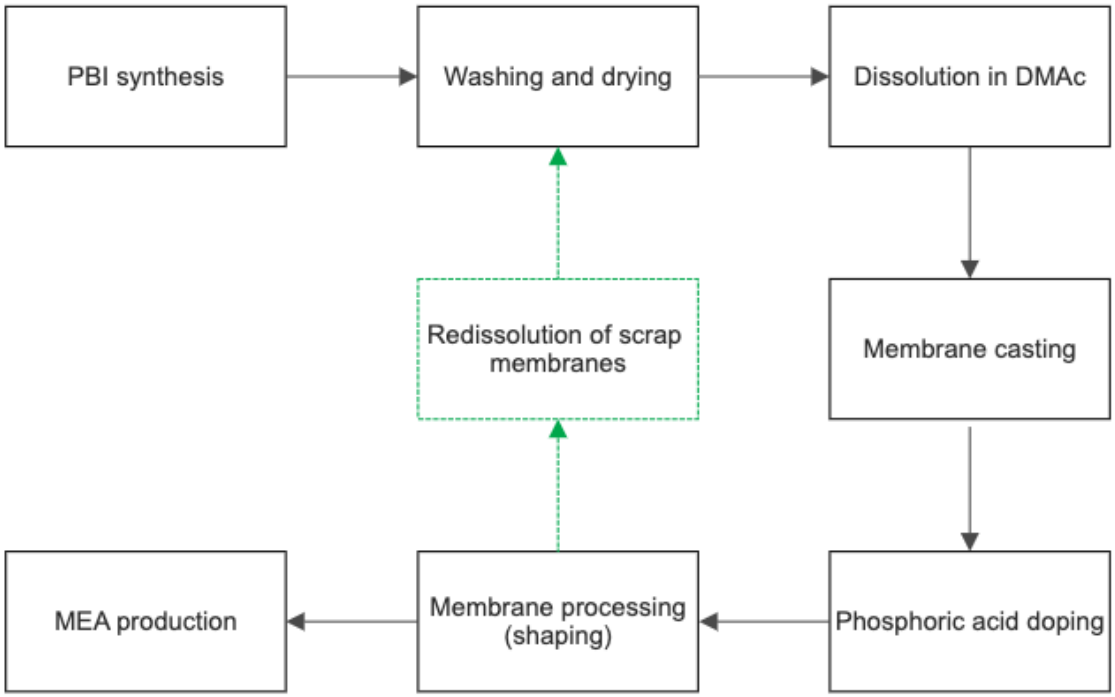

Figure 3.3: Flow chart schematic displaying the membrane production line at BWT including the suggested recycling process marked with dashed green lines.

The attempted recycling method (marked with green dashed lines in Figure 3.3) in the present work recovers the scrap PBI membranes by redissolving them in PPA or PA. In theory, the redissolution could be skipped in order to save a processing step. However, previous experience from BWT has concluded that the removal of the doping acid from the scrap membranes is highly difficult due to the different sizes and shapes of the scrap that are acquired. By redissolving the scrap before the washing process is initiated, the PBI is obtained in a precipitated state similar to the one from the synthesis of pristine PBI. The washing procedure allows the acid in the precipitated PBI to be effectively removed. Currently, there is ongoing research at BWT that involves shredding of the scrap membranes into small fragments to facilitate the acid removal so that the redissolution process can be avoided. However, in the present work it was decided to include this step to ensure complete removal of the doping acid. The PBI that is obtained from the redissolution can be re-fed into the production line by applying the same processing steps as for the pristine PBI starting with the washing procedure. By applying the recycling process, the production volume of pristine PBI can be reduced which would be beneficial from both an economical and environmental perspective.

4. Characterization of PBI

The purpose of this section is to give a brief description of methods and techniques that are used in this work to characterize PBI and the membranes that are cast from it. The profoundness of the given descriptions will be kept to what is deemed necessary for the reader to understand the purpose of the methods and how they are applied in the project at hand. As such, the reader is referred to other literature if a deeper theoretical understanding is required.

4.1 Molecular weight

The molecular weight is an important characteristic of polymers since there is a strong correlation between the molecular weight and physical properties such as mechanical strength, solubility and solution viscosity [18]. By controlling the molecular weight, these properties can be controlled according to the requirements for the specific application. There are several different techniques to determine the molecular weight. Some give absolute measurements, e.g. light scattering, but these are not always appropriate to use since they are time consuming and unpractical in every day work. In such situations it can be more suitable to estimate the molecular weight by a non-absolute method and correlate with data recorded from absolute methods [18]. It is important to note that the use of a non-absolute method for determining the molecular weight must always be supported by theoretical models that have been deduced from absolute measurement methods.

4.1.1 Viscometry

A convenient method for estimating the molecular weight of a polymer is to dissolve it and measure the viscosity of the resulting polymer solution. This method is called viscometry and is commonly used since it provides relatively accurate results while being of low labor intensity. Since PBI has a poor solubility in common organic solvents, 96-98% sulfuric acid is commonly used to dissolve PBI in viscometry measurements. The concentration of the polymer solution must be low to achieve accurate measurements and a solid content of 2-5 g L^{-1} is recommended [41]. The measurement is usually carried out using an Ubbelohde viscometer. This device works by pumping the polymer solution into a small reservoir. From there it flows by gravity within a capillary tube into a larger reservoir where it is collected. The time that it takes for the solution to pass between two pre-determined marks on the capillary tube is noted. The measured flow time is compared to the one of the pure solvent and the correlation between these can be related to the viscosity of the solution. Two different viscosity values can be calculated from the flow time difference, namely the relative viscosity η_{rel} (Eq. 4.1) and the specific viscosity η_{sp} (Eq. 4.2), where t is the flow time of the polymer solution and t_0 is the flow time of the pure solvent.

Eq. 4.1

$$\eta_{rel} = \frac{t}{t_0}$$

Eq. 4.2

$$\eta_{sp} = \frac{t - t_0}{t_0}$$

By measuring the specific viscosity at a range of different concentrations of the polymer solution and then dividing the specific viscosities with their respective polymer solution concentration *c*, the reduced viscosity η_{red} is obtained. If the reduced viscosity is plotted against the concentration and extrapolated to zero concentration, the intrinsic viscosity, $[\eta]$, can be calculated according to (Eq. 4.3), where *k* is the Huggins constant.

Eq. 4.3

$$\frac{\eta_{sp}}{c} = \eta_{red} = [\eta] + k \cdot [\eta]^2 \cdot c$$

Alternatively, the intrinsic viscosity of *m*-PBI may be estimated from a single-point measurement according to (Eq. 4.4), which has proven to be more than 99% accurate for low polymer solution concentrations [42].

Eq. 4.4

$$[\eta] = \left(\eta_{sp} + 3 \cdot ln\left(1 + \eta_{sp}\right)\right)/4 \cdot c$$

Finally, the inherent viscosity may be obtained from the ratio of the natural logarithm of the relative viscosity and the concentration (Eq. 4.5). This measurement is useful when comparing different polymer batches since it eliminates the effects of different measurement procedures. The inherent viscosity may also be determined from a single point measurement but the concentration should be specified.

Eq. 4.5

$$\eta_{inh} = ln(\eta_{rel})\,/c$$

The intrinsic viscosity may be related to the weight-average molecular weight, $\bar{M}_w$, by using the Mark-Houwink equation (Eq. 4.6).

Eq. 4.6

$$[\eta] = K \cdot \bar{M}_w{}^{\alpha}$$

K and α are empirically determined Mark-Houwink constants that are dependent on the range and the distribution of molecular weight that has been examined. Two sets of Mark-Houwink constants are commonly used for PBI dissolved in sulfuric acid. One set was reported by Buckley et al. [21] who made a three-data point measurement in the intrinsic viscosity region of 0.30-1.02 dL g^{-1} by light scattering measurements. The other set reported by Yuan et al. [42] was also obtained from light scattering but contained a broader data set in the region of 0.32-1.26 dL g^{-1}.

Table 4.1: Values of the Mark-Houwink constants K and α reported in literature by Buckley et al. [21], [42] *and Yuan et al.* [42] *respectively.*

	K (dL g^{-1})	α
Buckley et al.	1.94×10^{-4}	0.791
Yuan et al.	4.7×10^{-5}	0.93

4.2 Structural analysis

When working with polymers, it is of interest to identify and confirm the structure of the repeat unit. For this purpose, spectroscopical methods such as Nuclear Magnetic Resonance spectroscopy (NMR) and Infrared-Red spectroscopy (IR) are powerful tools. Extensive analysis of PBI and its derivatives have been employed using these methods and there are several research papers available in the literature regarding the subject [43]–[46].

4.2.1 Fourier-transform Infrared spectroscopy

Fourier-transform Infrared spectroscopy (FT-IR) is a technique that is used to characterize materials according to the infrared spectrum of absorption or emission. FT-IR is advantageous in certain applications due to its ability to effectively produce data over a wide spectral range. It can be used to identify and characterize polymers since the IR active groups in the polymer chains absorb as they were localized groups in single molecules. IR spectroscopy is frequently used in combination with Attenuated Total Reflectance (ATR) which is a method that allows samples to be directly examined in the liquid or solid state.

4.2.2 Nuclear Magnetic Resonance spectroscopy

Similarly, NMR may be applied for structural identification of the polymer repeat unit but it can also be used for calculating ratios of functional groups present in the structure. ^{1}H NMR is frequently used but ^{13}C NMR can also be useful in certain instances. For PA doped PBI, ^{31}P NMR may also be applied to study the interaction between the PA and the PBI and the conductivity mechanisms, as done by Hughes et al. [43]. The operation conditions for NMR analysis require that the polymer at hand is dissolvable in a deuterated solvent. For PBI, the choice of solvent is usually deuterated DMSO (DMSO-d_6) as it has been found to produce the most consistent results compared to e.g. deuterated sulfuric acid (D_2SO_4).

4.3 Phosphoric acid uptake

An important consideration in regard to membrane doping is the uptake of acid by the membrane. A high acid uptake leads to a high proton conductivity, but this comes at the cost of a lowered mechanical strength as the presence of acid has a plasticizing effect on the polymer - making it softer and weaker. As such, it is of great importance to find an optimal acid uptake

to balance these properties. The acid uptake is defined as the ratio between the PA content of the doped membrane and PBI content of the dry polymer. It can be calculated according to Eq. 4.7, where W_{PA} and W_{PBI} are the weight fraction of the acid-doped- and dry membrane respectively.

Eq. 4.7
$$AU = 100\,\% \cdot \frac{W_{PA}}{W_{PBI}}$$

The acid doping level (ADL) is commonly reported and is defined as the number of PA molecules per repeat unit of PBI (Eq. 4.8).

Eq. 4.8
$$ADL = \frac{W_{PA}}{M_{PA}} \Big/ \frac{W_{PBI}}{M_{PBI}}$$

M_{PA} and M_{PBI} are the molar masses of PA (97.99 g mol^{-1}) and *m*-PBI (308.34 g mol^{-1}) respectively. As the definition includes the molar mass of PBI, it is not possible to make direct comparisons between the acid doping level of different PBI chemistries as the molar mass varies.

The acid uptake of PBI membranes causes swelling that alters their dimensions. Due to the hydrophilicity of PBI there may also be a significant amount of water uptake that also contributes to the swelling effect. As the thickness of the membrane affects the proton conductivity and the mechanical strength [47], it is important to determine the degree of swelling. By measuring the dimensions before and after doping the swelling can be calculated on a linear, areal or volume basis by using (Eq. 4.9), where D_{doped} and $D_{undoped}$ are the dimensions of the doped and the undoped membrane respectively. It should be noted that the degree of swelling can vary in the three dimensions depending on how the membrane has been processed. For an example, extrusion of the polymer before casting can lead to anisotropic swelling as it causes the polymer chains to be oriented in the screwing direction of the extrusion machine.

Eq. 4.9
$$Swelling\,\% = 100 \cdot \frac{(D_{doped} - D_{undoped})}{D_{undoped}}$$

4.4 Thermal stability

An important property when considering the suitability for a material in PEM applications is its thermal stability – the relevancy is naturally further increased for high temperature operation applications. Thermogravimetric analysis (TGA) is commonly used to investigate thermally caused degradation processes and is performed by recording the weight loss or the normalized weight loss when a sample is heated in a furnace [18]. TGA can be run in isothermal mode, i.e. by applying a constant temperature, but it is most common to use a temperature ramping program that increases the temperature at a continuous rate.

When analyzing TGA data it is important to consider the conditions which the experiment is performed under. The extent of the degradation depends on what atmosphere the measurement

is performed under. Full oxidation into gaseous species is observed in presence of air, while there is significant soot formation when it is performed under an inert gas. The heating rate also influences the appearance of the TGA curve since the degradation process is time dependent. The temperature when 5 % ($T_{d5\%}$) or 10 % ($T_{d10\%}$) weight loss is observed is frequently reported in order to make comparisons between different materials.

4.5 Mechanical strength

As earlier mentioned, sufficient mechanical strength is essential for the membranes to tolerate the processing conditions when fabricating the MEA. It is also crucial for obtaining durability of the cell system during operation. The mechanical properties of the doped membrane is significantly lowered when PA is introduced into the PBI matrix since it reduces the intermolecular forces between individual polymer chains due to swelling of the membrane [1]. When the PA content of the doped membrane is low (ADL < 2), the mechanical properties of the membrane is largely unchanged. Although there is considerable swelling, this is compensated for by the hydrogen bonding between the PA and the benzimidazole groups [40]. However, the contributions to the mechanical strength of this interaction is overwhelmed by the plasticizing effect when the ADL is further increased.

4.5.1 Tensile testing

The mechanical strength of membrane samples is commonly evaluated by tensile testing. This method is performed by mounting a sample of known dimensions between two grips and measuring the force F needed to stretch the material, which is recorded as a function of the elongation of the sample. From this information it is possible to calculate the stress σ and strain ε which are defined in Eq. 4.10 and Eq. 4.11 respectively.

Eq. 4.10
$$\sigma = \frac{F}{w_0 \cdot d_0}$$

w_0 and d_0 are the initial width and thickness respectively before the sample deformation has begun.

Eq. 4.11
$$\varepsilon = \frac{L - L_0}{L_0}$$

L is the length of the sample at a certain applied force and L_0 is the initial length of the sample.

By plotting the stress against the strain, a stress-strain curve is attained. From this plot several important mechanical features can be extracted including the elastic modulus, yield stress, ultimate tensile strength as well as stress and elongation at break. In the application of PEMs in fuel cells, the elastic modulus is of special interest as it describes how the sample resists elastic deformation [41].

4.6 Proton conductivity

The proton conductivity is an essential property for the purpose of the PEM. By using Ohm's law the resistance of a membrane sample can be determined by measuring the voltage drop when a current is passed through it. The proton conductivity can then be determined from Pouillet's law (Eq. 4.12) which relates the resistance R to the product of the resistivity ρ and the ratio of the distance between the electrodes L and the cross-sectional area A of the sample.

Eq. 4.12

$$R = \rho \cdot \frac{L}{A} = \frac{1}{\sigma} \cdot \frac{L}{A}$$

The conductivity σ can be expressed as the reciprocal of the resistivity and as such the expression shows that a high conductivity and a low film thickness leads to a lower resistance. However, this relation is only valid for samples with a uniform cross section. It is therefore of great importance that the thickness of the membrane is constant over the entire sample.

4.6.1 Four-probe conductivity cell

The proton conductivity can be measured using a four-probe cell which is a system designed to eliminate the effects of polarization and contact resistance. When two electrodes supply an electric current through the ionically conducting membrane, there is a polarization formed at the contact point due to a change in active species. The resistance generated by this polarization causes a non-wanted contribution to the overall resistance that is calculated from the measured voltage drop [41]. To prevent this, two additional electrodes with a fixed distance apart are introduced that only measure the voltage without supplying any current. The four-probe cell is placed within a sealed glass tube and may also be put in a furnace for temperature control. The humidity has a significant impact on the conductivity measurements and should be controlled and specified to be able to make relevant comparisons. The resistance can be measured in-plane by placing the current supplying and the voltage measuring electrodes on opposite sides of the membrane. Correspondingly, the trough-plane resistance is measured by attaching the electrodes of each electrode pair on opposite sides of the membrane. A common approach is to apply a high frequency symmetric square wave current to the current supplying electrodes [41]. The voltage drop between the two inner electrodes can be measured by using an oscilloscope and from that information the proton conductivity may be calculated according to the procedure described above.

5. Experimental

5.1 Pre-studies

To investigate the conditions required for the redissolution of scrap PBI membranes, a number of experiments were carried out where the influence of temperature, concentration and choice of solvent was examined by varying the different parameters. The scrap material that was used for these experiments came from several different PBI batches and were as such unsorted. This was done due to the limited amount of material available that belonged to the same batch which was deemed needed for further measurements and characterization. Consequently, the material that was used in these experiments contained a mix of PBI with different $\bar{M}_w$ which theoretically should lead to a broadening of the molecular weight distribution. This is detrimental in the purpose of producing PEMs as it may cause variation of the properties across the membrane. Thus, the experiments at hand were solely carried out with the purpose of investigating the effects of different re-dissolution conditions. The results of the experiments were mainly evaluated based on solubility but also practical manageability and visual appearance of the resulting PBI.

5.2 Redissolution of membranes

Scrap membrane parts were collected and cut into small pieces to prevent material from getting stuck to the mechanical stirrer and to the side of the walls of the reaction vessel. The pieces were added to the solvent in a 2 L glass round-bottom flask and heating and mechanical stirring (12 Hz) was applied. The re-dissolution was performed for 24 h under a nitrogen atmosphere to eliminate the possible interference of oxygen, although depending on the operating conditions, less time than that was sometimes required to visibly achieve full dissolution. After the membranes had dissolved, the PBI was precipitated by pouring out the solution in a large tank filled with distilled water.

5.3 Washing and drying

The PBI was washed according to the following procedure with the purpose of removing all of the acid residues from the PBI matrix in order to make it dissolvable in DMAc. The first step of the procedure was performed by submerging the PBI in hot water for 24 h in order to wash out the bulk of the acid residues from the polymer matrix. Thereafter, the PBI was washed in a sodium hydroxide solution for an extended time period. The pH of the solution was measured continuously to confirm that it was kept constant to ensure that all acid was removed. Finally, it was submerged in hot water again to neutralize the polymer. The neutralization process was evaluated by measuring the conductivity of the process water using a conductometer. The water was continuously changed until a sufficiently low conductivity measurement was achieved. When the washing procedure was completed, the PBI was grinded into a fine powder before it was dried at 130 °C to evaporate the water that had been absorbed during the washing procedure.

5.4 Membrane preparation

The reprocessed PBI membranes were hand-casted by using the organic solvent evaporation method. After the PBI powder had been thoroughly dried to prevent solvent hydrolysis it was dissolved in DMAc to produce a casting solution. The dissolution was performed under atmospheric pressure and by slowly increasing the temperature of the solution up to a maximum of 70 °C. The resulting solution was filtered using a syringe equipped with a 1 μm filter to remove undissolved particles.

The membrane casting was performed by pouring the solution on to glass petri dishes with diameters of 19.7 cm that were then heated in an oven. To promote a slow evaporation of the solvent, the temperature was first set to 80 °C for 3 h and then further increased to 120 °C for 21 h. After removal, the membranes were covered in tissues drenched in cold water to facilitate the delamination from the substrates. Thereafter, they were submerged in hot distilled water for 2 h to wash out DMAc residues before being dried at 80 °C under vacuum. Acid doping was performed by submerging the membrane samples in 85 wt.% PA inside of closed plastic containers. The doping process was carried out over 72 h at room temperature in order to reach acid doping equilibrium.

5.5 Characterization

The weight average molecular weight was estimated from viscometry using the Mark-Houwink constants reported by Buckley et al. ($K = 1.94 \times 10^{-4}$, $\alpha = 0.791$) [21]. The measurements were performed using an Ubbelohde viscometer at 30 °C and with a polymer solution concentration of 5 g L^{-1}. The PBI was dissolved in 96% sulfuric acid under gentle heating and stirring in a water bath until full dissolution was achieved. Three replicates were produced for each sample to provide statistical calculations.

Structural analysis of the PBI samples was performed using ^{1}H NMR spectroscopy and ATR FT-IR. ^{1}H NMR spectra were obtained using a Magritek SpinSolve 80 MHz spectrometer using deuterated dimethylsulfoxide (DMSO-d_6) as the solvent. The chemical shifts are presented in ppm and given relative to the solvent peak at 2.50 ppm. ATR-FTIR was performed using a Perkin Elmer Spectrum Two equipped with an universal ATR sampling accessory in the frequency range from 4000 – 500 cm^{-1}.

ADLs and the corresponding volume swelling were calculated, based on the dry membrane weight and dimensions, using Eq. 4.8 and Eq. 4.9 respectively. The dimensions and weight were recorded before and after acid doping. As the doping process leads to uptake of both water and acid, the samples were dried at 80 °C under vacuum until a constant weight was achieved which was assumed to remove the water present in the samples. However, any residual water in the samples would lead to an overestimation of the acid uptake and ADL.

TGA was carried out on an Netzsch STA 449. The temperature was increased from room temperature to 800 °C at a rate of 10 °C min^{-1} in air. Measurements were performed on undoped

membrane samples and the sample weight was roughly 10 mg. The weight loss was normalized against the weight of the membranes at 200 °C to eliminate the contributions of absorbed water.

The tensile properties of the doped membranes at room temperature in air were determined from stress-strain curves obtained from a Mecmesin ILC Load Cell 50N. Three samples of each membrane were cut into rectangular strips of 10 mm × 30 mm. A constant cross-head speed of 10 mm min^{-1} was used. The engineering stress was calculated by using the initial cross-section area of the samples.

The in-plane proton conductivity was characterized using a four-probe conductivity cell in the temperature range of 100-160 °C with increments of 20 °C. The dimensions of the samples were recorded at room temperature and the thermal expansion was assumed to be negligible. The width of the samples was 10 mm and an average for the thickness was taken by measuring it at five points across each sample. Platinum foil was used for the current supplying electrodes. For the voltage measuring electrodes, platinum probes were used that were fixed with a distance of 1 cm apart. The samples were mounted into the cell right after gently blotting the membrane surface with filter paper to remove any excess acid. Measurements were performed under air without any humidification and the cell was placed inside a furnace for temperature and humidity control.

5.6 Fuel cell testing

Gas diffusion electrodes for fuel cell testing were provided by BWT. The cathode and the anode had Pt/Co and pure Pt catalysts respectively, with a platinum loading of 1.0 mg cm^{-2}. The active area of the cell was 21 cm^2. MEAs were assembled by sandwhiching the membranes between the two electrodes and hot pressing them at 100 °C for 3 minutes. Reformed hydrogen and air were fed to the anode and cathode respectively at a stoichiometry of λ_{H2} = 1.5 and λ_{Air} = 2.5. Testing was carried out over 48 h at 160 °C and a constant current density of 0.4 A cm^{-2}. Polarization curves were obtained after 5, 24 and 48 h of operation by recording the voltage after two minutes at a specific current density.

6. Results and discussion

6.1 Reprocessing of scrap PBI membranes

The different redissolution conditions that were attempted on the unsorted PBI membranes are summarized in Table 6.1. The observations made from the experiments were noted and can be found as qualitative comments in Table 6.1.

Table 6.1: The table displays the different conditions that were attempted for the redissolution of scrap PBI membranes. The parameters that were investigated included temperature T, concentration c (reported in wt.% on the doped membrane basis) and the choice of solvent. Time was 24 h for all experiments. In the table, qualitative comments based on observations from each experiment are found.

Experiment	T (°C)	c (wt.%)	Solvent	Comments
1	100	12	PA	No observed solubility.
2	140	12	PA	Low solubility with significant lump formation.
3	180	12	PA	High solubility. Precipitation yielded soft PBI strands.
4	180	5	PA	High solubility. Precipitation yielded a slush-like substance that was difficult to collect.
5	180	17	PA	High solubility. The solution was highly viscous to the point that it was much difficult to precipitate.
6	100	9	PPA	Slow dissolution. After 24 hours there were no visibly undissolved membrane parts left.
7	140	12	PPA	High solubility. Precipitation yielded PBI strands that were visually similar to pristine PBI.
8	140	17	PPA	High solubility. The solution was highly viscous to the point that it was much difficult to precipitate.
9	180	12	PPA	High solubility. Precipitation yielded PBI strands that were visually similar to pristine PBI.
10	210	14	PPA	High solubility.

From the observations made from the experiments seen in Table 6.1, it was concluded that the washed and cleaned PBI scrap displayed little to no solubility at temperatures between 100-140 °C when 85 wt.% PA was used as the solvent. This is explained by the fact that the solubility of PBI in PA is relatively poor and lower than what it is in PPA. However, when PA is heated up to 180-200 °C there is significant condensation taking place with formation of acid anhydrides and eventually PPA [41]. Consequently, the solubility drastically increased when the solution was heated to 180 °C or above. In the experiments using PPA as the solvent the solubility was high for the entire temperature range that was tested and the PBI membranes were fully dissolved even at the lowest attempted temperature (100 °C), however, the dissolution rate noticeably increased with the temperature.

Regarding the concentration of the solution, it was noted that 12 wt.% on the doped membrane basis, gave a polymer solution that precipitated in the form of strands similar to what is seen in the synthesis of pristine PBI. The lowest attempted concentration precipitated as a slush-like substance that could not be collected with ease. On the contrary, the highest attempted concentration made the solution highly viscous to the point that it was much difficult to pour it out from the glass flask which led to a loss of material. Based on the observations, the most suitable conditions were deemed to be 180 °C and a concentration of 12 wt.%. These conditions were therefore applied to the redissolution of membranes from a single PBI batch with an intrinsic viscosity of 1.37 dL g^{-1} and a corresponding $\overline{M}_w$ of 73 000 g mol^{-1} calculated from the Mark-Houwink constants reported by Buckley et al. (see Table 4.1). The influence of the choice of solvent was decided to be investigated further since the visual appearance of the precipitated PBI varied between the two alternatives, see Figure 6.1. Additionally, it was deemed of interest to evaluate the quality and performance of the reprocessed PBI using PA and PPA as the respective solvent. Since PA is cheaper to purchase and may also be re-used from the doping process, it would provide a more economical and sustainable option. One experiment each was carried out with PPA and PA using the selected conditions. The samples from these experiments will from here on be referred to as **PBI-PPA** and **PBI-PA** respectively. Pristine samples from the original batch were also prepared for comparisons and these samples will be referred to as **PBI-Ref**.

*Figure 6.1: PBI powders after re-dissolution and subsequent washing and drying. **PBI-PPA** and **PBI-PA** are shown to the left and right respectively.*

6.2 Viscometry measurements

After washing and drying, the viscosity of **PBI-PPA** and **PBI-PA** and the corresponding $\bar{M}_w$ were calculated. Additionally, a membrane sample from the reference material was de-doped by washing it in a sodium hydroxide solution. The $\bar{M}_w$ of this sample, **PBI-UD,** was measured to investigate if the redissolution and the subsequent washing procedure had an influence on the $\bar{M}_w$. The inherent viscosity was calculated from a single point measurement using Eq. 4.5. and the intrinsic viscosity was estimated according to Eq. 4.4. The estimated intrinsic viscosity was then used to calculate $\bar{M}_w$ using the Mark-Houwink equation (Eq. 4.6). The Mark-Houwink constants were taken from the light-scattering measurements reported by Buckley et al. [21]. It should be noted that these constants were determined from a three-point measurement in the low intrinsic viscosity region of 0.30-1.00 dL g^{-1}. As the intrinsic viscosities of the examined samples were all outside of this region, the estimation of $\bar{M}_w$ might be inaccurate. The results are presented in Table 6.2.

Table 6.2: The inherent viscosity n_{inh}, intrinsic viscosity [n] and the weight average molecular weight $\bar{M}_w$ calculated using the Mark-Houwink constants reported by Buckley et al. [21] *and Yuan et al.* [42].

Sample	η_{inh} (dL g^{-1})	[η] (dL g^{-1})	$\bar{M}_{w,Buckley}$ (g mol^{-1})	$\bar{M}_{w,Yuan}$ (g mol^{-1})
PBI-UD	1.17 ± 0.026	1.27 ± 0.032	67 000 ± 2 000	58 000 ± 1 000
PBI-PPA	1.14 ± 0.042	1.24 ± 0.051	65 000 ± 3 000	57 000 ± 2 000
PBI-PA	1.09 ± 0.097	1.18 ± 0.116	61 000 ± 6 000	53 000 ± 5 000

As can be seen in Table 6.2, the intrinsic viscosities for the three different samples were in the range of 1.18-1.27 dL g^{-1}, corresponding to a $\bar{M}_w$ of 61 000-67 000 g mol^{-1} when using the same Mark-Houwink constants as for the reference material. By applying the constants reported by Yuan et al. [42], a lower range of 53 000-58 000 g mol^{-1} are instead obtained – which could be a more accurate estimation since these constants were calculated from an intrinsic viscosity region closer to the one in the present work. The former values can be compared to the $\bar{M}_w$ of the pristine reference material that was 73 000 g mol^{-1}. Of the different sample series none had a standard deviation that covered the $\bar{M}_w$ of the original batch. As such it is possible that the redissolution process had an effect on lowering the $\bar{M}_w$. Reduction of the molecular weight of polymers may happen due to degradation which can be caused by several different phenomena, e.g. thermal, chemical or mechanical degradation. The well-documented thermal and chemical stability of PBI makes thermal and chemical degradation unlikely to occur. However, it is plausible that structural defects in the polymer backbone – such as incomplete ring closure in some units (see Figure 3.2) – could cause weak amide bonds that easily break by hydrolysis during the redissolution. The suggested mechanism would reasonably be enhanced when using

PA as the solvent due to the substantial presence of water and could explain why this sample displayed the largest deviation from the $\bar{M}_w$ of the pristine reference material. Additionally, mechanical degradation can occur when a polymer is dissolved in a solvent and exposed to powerful shearing forces due to vigorous stirring [48]. Although it is improbable that the conditions that the experiments at hand were performed under would be sufficient to cause such an effect. Experimental errors could also affect the viscosity measurement as it is sensitive to deviations in the polymer solution concentration. Nevertheless, the obtained $\bar{M}_w$ for all samples was in the range that allows for casting of mechanically robust PBI membranes when doped with an ADL of ~10-12 which is required to attain sufficient proton conductivity [24].

6.3 NMR and FT-IR spectra

^{1}H NMR spectra for all samples with the corresponding proton assignment in the PBI repeat unit can be found in Figure 6.2. By comparing the spectra of **PBI-PPA** and **PBI-PA** with that of **PBI-Ref** it can be confirmed that the chemical structure of the PBI remains unchanged after reprocessing. It also aligns with ^{1}H NMR analysis in the literature such as the one reported in [44]. The peak at 13.2 ppm belongs to the imidazole proton and the peaks at 9.2-7.7 are assigned to the aromatic protons in the structure [44].

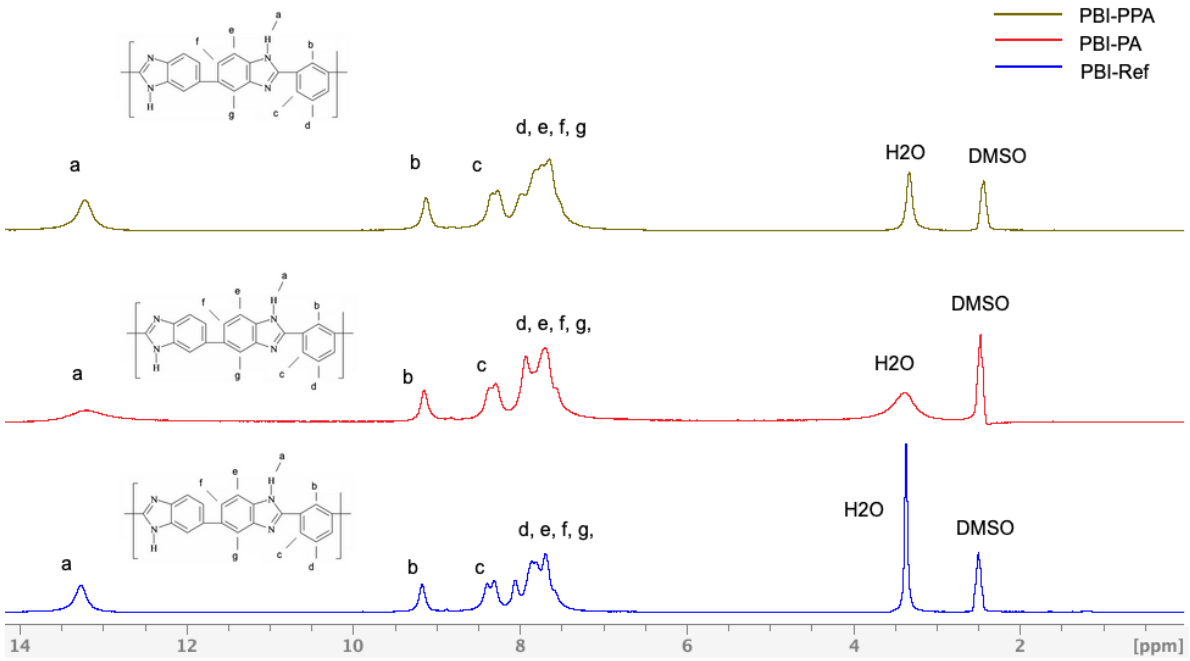

Figure 6.2: ^{1}H NMR spectra for PBI samples dissolved in DMSO-d_6.

The FT-IR spectra of the undoped membrane samples are seen in Figure 6.3. The region of 2000 – 4000 cm^{-1} is where the stretching of N-H bonds is displayed. According to Musto et al [45], the peak in the spectrum at 3410 cm^{-1} is assigned to the stretching vibrations of 'free', non-hydrogen-bonded N-H groups while the weak peak observed at 3145 cm^{-1} is attributed to self-associated, hydrogen-bonded N-H groups. Another characteristic region for PBI is observed at the frequency range of 1650-1500 cm^{-1} which includes a peak at 1612 cm^{-1} that is assigned to the stretching vibrations of C=C/C=N bonds and peaks at 1536 and 1440 cm^{-1} that corresponds to the in-plane deformation of the benzimidazole unit [49].

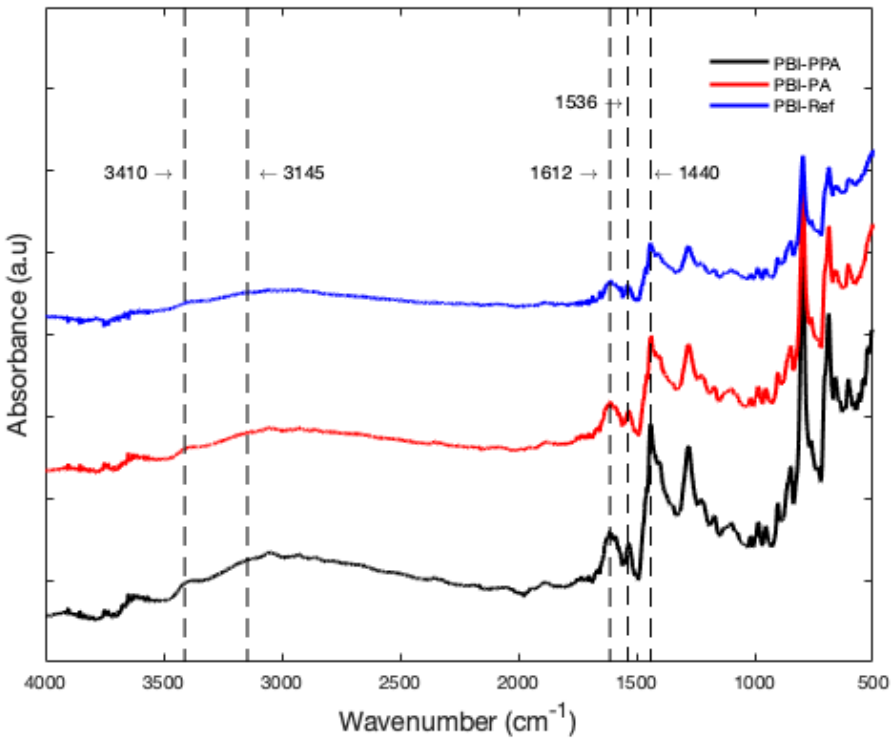

Figure 6.3: ATR FT-IR spectra for undoped PBI membranes at room temperature. The dotted lines marks the wavenumber for a few characteristic regions of PBI.

6.4 Membrane casting and acid doping behavior

The obtained PBI powders were readily dissolved in DMAc according to the procedure described in 5.4 Membrane preparation. An 8.6 wt.% casting solution was first prepared but due to considerable variations of the membrane thickness after casting - which was assumed to be enhanced by the high viscosity - it was decided to dilute the solution to 5 wt.% to facilitate an equal distribution over the substrate surface. At this concentration the homogeneity of the thickness was improved and was roughly 40 µm.

The obtained PA uptake, ADL and swelling ratio after doping in 85 wt.% PA are presented in Table 6.3. The ADL for **PBI-PPA, PBI-PA** and **PBI-Ref** was found to be 10.7, 10.4 and 10.5 respectively. According to the work by Yang et al. [24], the ADL of high molecular weight PBI is in the range of 10-12 when doped in 85 wt.% PA. They also reported that the time to reach acid doping equilibrium increases with increasing molecular weight. In the present work, the PBI membranes were immersed in PA for 72 h which was assumed to be sufficient to reach equilibrium. While the measured ADLs were within the expected range for high $\bar{M}_w$ PBI doped in 85 wt.% PA - it should be noted that the doping procedure was not performed under a humidity controlled environment. It is plausible that the hygroscopic PA could have absorbed moisture from the surrounding air which would effectively cause a reduction of the PA concentration which in turn would reduce the acid uptake since it is concentration dependent. The volumetric swelling ratio for the samples displayed a larger disparity and was determined to be between 168-204%. The reported volume swelling of PBI membranes in the literature is also somewhat inconsistent and it varies between 150-250% when the ADL is between 10-11

[50]. This is likely explained by the difficulties in accurately measuring the dimensions of the swollen membranes due to their softness. For an example, the membranes may be significantly compressed when they are wiped off to remove excess acid. Nevertheless, the obtained volume swelling ratios are in relative proximity to the ones reported for high molecular weight PBI membranes [24], that generally display a less prominent swelling due to the longer molecular chains which makes the polymer more resistant to rearrangement.

Table 6.3: Acid uptake (AU), acid doping level (ADL) and the volumetric swelling ratio of PBI membranes doped in 85 wt.% PA at room temperature.

Sample	AU(wt.%)	ADL (H_3PO_4/PBI_{ru})	Swelling (vol.%)
PBI-PPA	342 ± 12	10.7 ± 0.4	180 ± 18
PBI-PA	327 ± 7	10.4 ± 0.2	168 ± 13
PBI-Ref	328 ± 9	10.5 ± 0.2	204 ± 23

Using ATR FT-IR (*Figure 6.4*) acid doping was confirmed by the presence of the broad N-H stretching absorption band in the region of 2500-3600 cm^{-1} [13] as well as the absorption band at around 1000 cm^{-1} that is attributed to the vibration of acid anion groups [33].

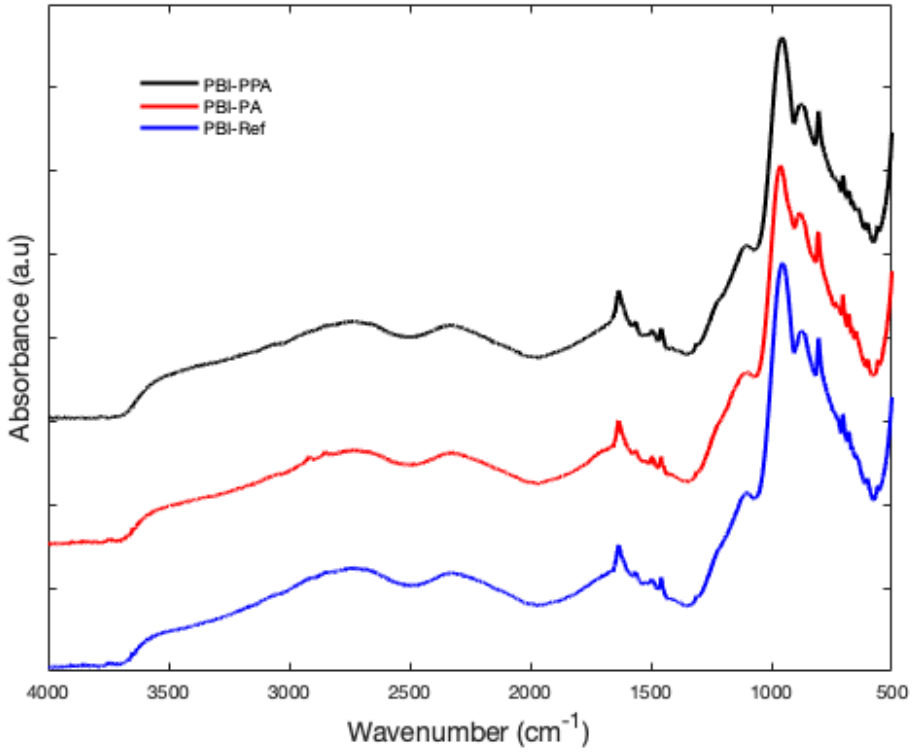

Figure 6.4: ATR FT-IR spectra for PBI membranes doped in 85 wt.% phosphoric acid

6.5 Thermogravimetric analysis

TGA was used to evaluate the thermal stability of the undoped reprocessed membranes, which was benchmarked against a pristine PBI membrane sample. As shown in Figure 6.5, the TGA curves all display a similar trend. All samples had an initial weight loss of ~7-10% starting from 100 °C which is attributed to the evaporation of absorbed water molecules. Since this information is not of interest in the investigation at hand, the weight loss was normalized against the respective weight of the samples at 200 °C at which point they were considered fully dry. The onset of thermal degradation was observed around 400 °C for all samples. $T_{d5\%}$ was observed at 523 °C for the samples **PBI-PPA** and **PBI-Ref**. The corresponding value for **PBI-PA** was slightly higher at 547 °C. The decomposition rate increases significantly at roughly 550 °C due to the degradation of the polymer backbone. As the temperature reaches 700 °C, the PBI is fully oxidized into volatile species. The findings from the TGA measurement in the present work are in agreement to what has previously been reported for PBI [23]. As there is no significant difference in the thermal stability between the reprocessed samples and the reference it can be concluded that the reprocessing steps does not impact this property.

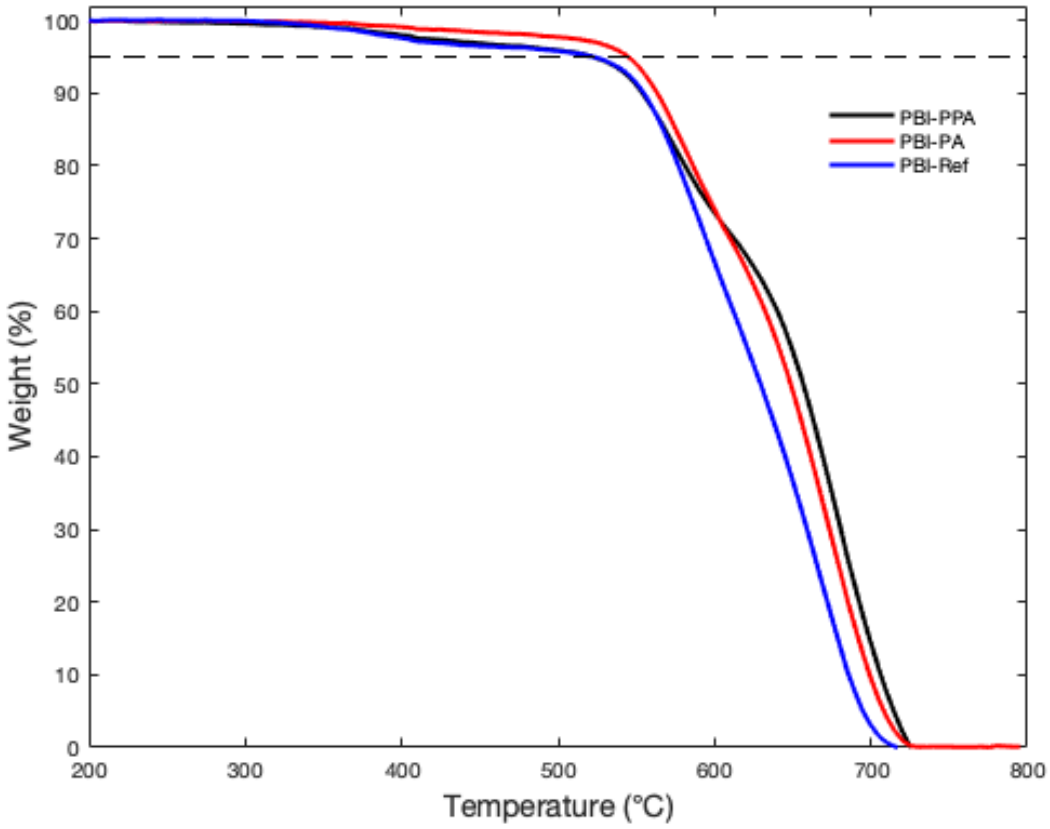

Figure 6.5: TGA curves for undoped PBI membranes. The curves have been normalized with respect to the weight at 200 ℃. The dotted line represents the 5% weight loss and the intercept of the TGA curves with this line gives $T_{d5\%}$.

6.6 Tensile properties

In Figure 6.6 representative stress-strain curves for the PA doped samples **PBI-PPA, PBI-PA** and **PBI-Ref** at room temperature are displayed. The corresponding average tensile properties of three samples of each test series are presented in Table 6.4.

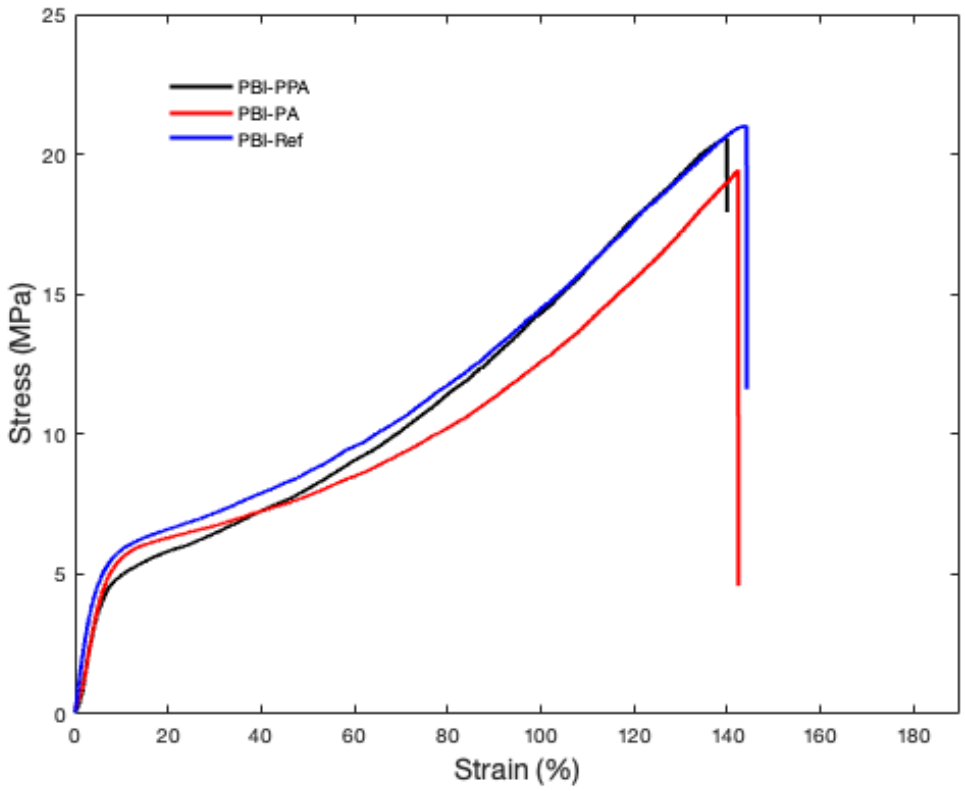

Figure 6.6: Representative stress-strain curves for PA doped membranes at room temperature. The corresponding $\bar{M}_w$ and ADL for each sample can be found in Table 6.2 and Table 6.3 respectively.

Table 6.4: The elastic modulus, tensile stress at break and elongation at break at room temperature for doped PBI membranes. The values have been calculated from three duplicates for each set. The stress-strain curves for each set are found in Appendix A.

Sample	Elastic modulus (MPa)	Tensile stress at break (MPa)	Elongation at break (%)
PBI-PPA	120 ± 20	19.2 ± 1.4	151 ± 17
PBI-PA	110 ± 30	19.3 ± 4.2	132 ± 23
PBI-Ref	120 ± 10	20.4 ± 1.8	150 ± 14

As seen in Table 6.4, the measured tensile strength at break for **PBI-PPA** and **PBI-PA** was 19.2 and 19.3 MPa respectively, which was slightly lower than the corresponding value for **PBI-Ref**

which was 20.4 MPa. It is well established that the mechanical strength of polymers depend on the molecular weight since an increase in the polymer chain length leads to more chain entanglements [18]. Hence, the tensile strength and the elastic modulus is improved when increasing the molecular weight since more energy is required to break or disentangle the polymer chains. Furthermore, in the case of doped PBI membranes the mechanical properties also depend on the doping level [1]. As earlier discussed, the introduction of PA into the PBI matrix induces a plasticizing effect which makes the PBI more soft and viscous by reducing the intermolecular hydrogen bonding between polymer chains. Due to its relatively high $\bar{M}_w$, the reprocessed PBI in the present work display comparatively good mechanical properties when the corresponding ADL is taken into account. However, it is noted that the tensile strength at break is slightly low when comparing with previous reports in the literature for PBI with similar $\bar{M}_w$ and ADL. Yang et al. [24] reported tensile strength at breaks of ~25-30 MPa for PBI membranes with $\bar{M}_w > 55$ kg mol^{-1} and ADLs of ~10-12. An explanation for the disparity could be that the reprocessed membranes had some variation in the thickness, unlike the reference material that had a constant thickness. It is known that the tensile properties is heavily dependent on the presence of microscopic defects in the membranes. Because of the variations in the thickness in the reprocessed samples it is plausible that the reprocessed sample contains microscopic defects to a greater extent since the number of defects may change with the sample thickness [47]. Generally, the standard deviation for tensile tests is relatively high because of the mentioned presence of defects but also due to the sensitivity for how the sample is mounted in the testing equipment [41]. Another plausible explanation for the disparity could be that the thickness of each membrane sample was only measured at one point. Any deviations in the thickness across the sample would cause inaccuracy in the calculation of the tensile strength as seen from Eq. 4.10, and taking an average value for the thickness might have increased the accuracy of the measurements. Increasing the amount of replicates in the present work would likely have improved the precision but was not deemed possible due to the limited amount of available material. The elastic modulus and the observed elongation at break were roughly 120 MPa and 150% respectively for all samples which is in accordance with previous what has been previously reported [24], [50].

A more viable measurement of the mechanical strength in terms of MEA processing and operation in an actual HT-PEMFC system would have been obtained if the tensile testing was performed at an elevated temperature. This is because the mechanical strength is decreased when the temperature is increased towards the glass transition temperature (T_g). Below this temperature for a given polymer it behaves like a stiff and brittle material. However, when the temperature is increased above T_g, there is sufficient thermal energy for the individual polymer chains to move in relation to each other - making the polymer behave more viscous or rubbery [18]. In the undoped state, PBI possesses a very high T_g of above 400 °C [14] and the physical properties are largely unchanged at temperatures below this. The observed T_g is significantly lowered after acid doping because of the swelling-induced separation of the polymer chains. Hence, the mechanical strength of the doped membrane is drastically lowered when the temperature is increased. In the previously mentioned study by Yang et al. [24] the tensile strength at break for a PBI membrane ($\bar{M}_w$ = 78 kg mol^{-1}, ADL = 10.8) decreased from 30.3 MPa to 7.3 MPa when the temperature was increased from room temperature to 130 °C.

6.7 Proton conductivity

The proton conductivity under unhumidified conditions for PA doped membranes measured at a temperature range of 100-160 °C is shown in Figure 6.7 and the results are summarized in Table 6.5.

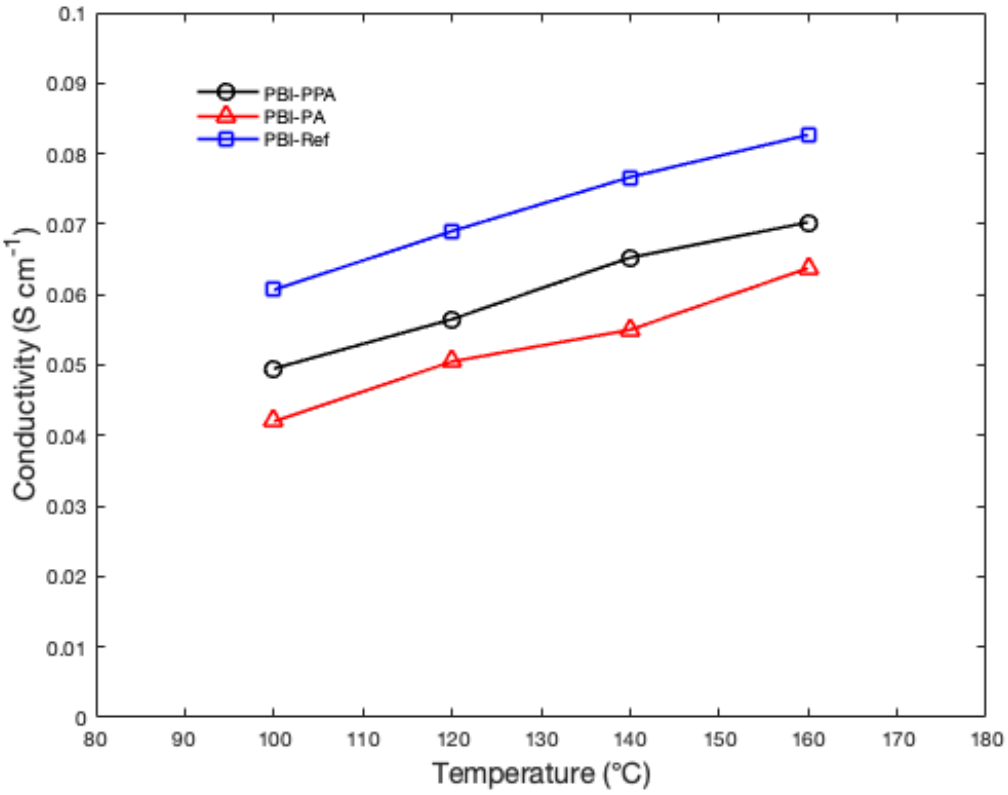

Figure 6.7: The proton conductivity under unhumidified conditions for PBI membranes doped in 85 wt.% phosphoric acid as a function of temperature.

From Figure 6.7, it is observed that the proton conductivity increases with the temperature as expected. Proton conductivity in acid doped PBI membranes is a thermally activated phenomena that follows the empirical Arrhenius equation and generally increases with the temperature. As reported in the literature [51], an exception is observed when the temperature reaches roughly 180 °C. In this temperature range there is significant condensation of PA into acid anhydride species which are less conductive than PA - thus, the increase in the proton conductivity is negligible when increasing the temperature from 160 to 180 °C.

The proton conductivity for the **PBI-PPA** and **PBI-PA** membranes at 160 °C was found to be 0.064 and 0.070 S cm^{-1} respectively, which was lower than the corresponding value for **PBI-Ref** which was 0.083 S cm^{-1}. Notably, the observed conductivity for the two reprocessed samples are lower in the entire examined temperature range in comparison to the reference. It is well established that the conductivity of PBI membranes is strongly correlated to the ADL. As previously described, the ADL of all the studied samples were observed to be approximately the same. Hence, very similar values for the conductivities would be expected. There are several plausible explanations for the observed disparity. Firstly, there could be inaccuracies in the

doping procedure as well as in the measurements of the ADL causing the observed values to deviate from the actual ADLs. As previously mentioned, the samples were not kept in a humidity controlled environment during doping and the subsequent post-doping storage which may have affected the ADL. Secondly, the calculations of the conductivity depend on the dimensions of the samples. In the present work, the dimensions were recorded at room temperature which means that the effect of thermal expansion was not taken into consideration. Furthermore, the thickness of the membrane was calculated as an average by measuring it at five points across its length. As the voltage drop is recorded between the two inner electrodes in the cell, a more accurate approach could have been to take the thickness as the one measured between these two points. The softness of the membranes also makes it difficult to get an accurate measurement without pressing the thickness gauge into the membrane. Lastly, the conductivity is significantly affected by the relative humidity. All measurements were performed inside a furnace where the temperature and the humidity were observed. However, it was noted that the relative humidity varied between 0.2-0.8% between the measurements also depending on the temperature inside the furnace.

Table 6.5: The proton conductivity under unhumidified conditions in the temperature range of 100-160 ℃ for doped PBI membranes. The average thickness of each sample in the doped state is shown in the second column. Corresponding ADLs for each membrane sample can be found in Table 6.3.

Sample	δ (μm)	$\sigma_{100\,°C}$ (S cm^{-1})	$\sigma_{120\,°C}$ (S cm^{-1})	$\sigma_{140\,°C}$ (S cm^{-1})	$\sigma_{160\,°C}$ (S cm^{-1})
PBI-PPA	89	0.050	0.057	0.065	0.070
PBI-PA	76	0.042	0.051	0.055	0.064
PBI-Ref	81	0.061	0.069	0.077	0.083

The calculated proton conductivities are generally in good agreement with what has been outlined in the literature for PBI with similar ADLs under the same conditions. For an example, Aili et al. [50] reported an in-plane anhydrous proton conductivity for the pure PBI membrane with an ADL of 11 that increased from 0.04 – 0.07 S cm^{-1} in the temperature range of 120-180 °C.

6.8 Fuel cell performance

One MEA each was prepared using membranes based on **PBI-PA** and **PBI-PPA**. These membranes were prepared by the same approach as previously with the difference being that it was stored in a humidity controlled cabinet (21-23%) during the doping process and therefore the ADL was re-measured for these individual samples. When preparing the MEA from **PBI-PA**, it is likely that the excess acid in the membrane was not sufficiently removed. This resulted in very poor performance in the fuel cell testing (see Figure 6.8 and Figure 6.10) – presumed to be caused by flooding of the gas diffusion electrodes by the excess acid. Since no more material was available from this sample series the testing could not be repeated. Therefore, the results from the fuel cell testing are solely based on a membrane from **PBI-PPA**. The thickness in the undoped state of this membrane was approximately 37 µm and the ADL was 10.2.

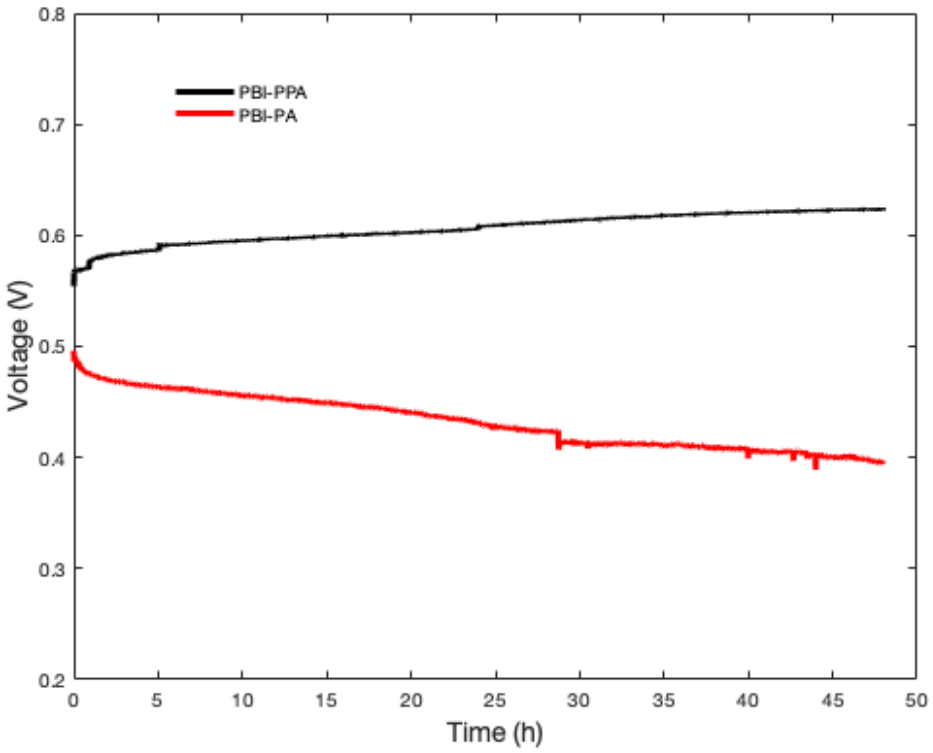

Figure 6.8: Cell voltages as a function of time during 48 h of operation. The operation temperature was 160 °C at a current density of 0.4 A cm^{-2}. The cells were fed with ambient pressure hydrogen and air at a stoichiometry of λ_{H2} = 1.5 and λ_{Air} = 2.5.

Fuel cell testing was carried out at 160 °C and a constant current density of 0.4 A cm^{-2} for 48 h. In Figure 6.8, the voltage evolution at 0.4 A cm^{-2} during the initial 48 h of the two MEAs using membranes from **PBI-PPA** and **PBI-PA** is displayed. As can be seen the performance of **PBI-PA** was significantly lower, as previously mentioned, and the voltage steadily decreases with time. For the **PBI-PPA** MEA the voltage instead increases from an initial value of 0.569 V to 0.624 V after 48 h of operation. The increase in voltage that is seen during this period is attributed to the activation of the fuel cell which is a process that is assumed to be caused by acid redistribution from the doped membrane to the catalyst layer [52]. The wetting of the

catalyst enhances the electrode kinetics which improves the fuel cell performance, hence, the observed increase of the cell voltage. If the testing would have been performed for a longer time period, it would have been observed that the cell voltage is stabilized at a certain value after the activation of the fuel cell has finished.

In Figure 6.9, the voltage evolution at 0.4 A cm^{-2} during the initial 48 h of the **PBI-PPA** MEA is compared to two commercial Dapozol® MEAs that have been classified to display high and low performance respectively. It can be observed that the performance of the **PBI-PPA** membrane is comparable to what is seen from Dapozol® MEAs. The initial voltage for the high and the low performance Dapozol® MEAs was 0.591 and 0.567 V respectively. The voltage after 48 h of operation for **PBI-PPA** (0.624 V) is similar to what is obtained from the high performance MEA that displayed a voltage of 0.628 V and notably higher than the 0.607 V that is exhibited from the low performance MEA. It should be taken into consideration that 48 h is a short time period in terms of issues such as wash out of PA, evaporation and catalyst dissolution. Consequently, conclusions regarding the long-term durability and performance cannot be drawn from this data and would require further testing.

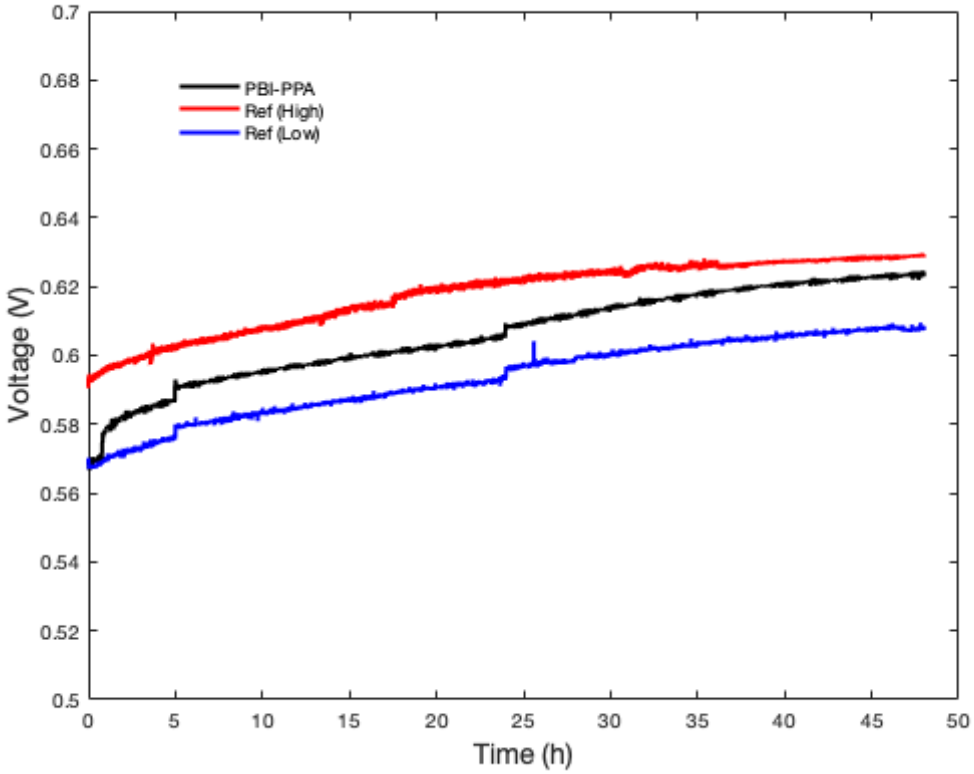

Figure 6.9: Cell voltages as a function of time during 48 h of operation. The operation temperature was 160 ℃ at a current density of 0.4 A cm^{-2}. The cells were fed with ambient pressure hydrogen and air at a stoichiometry was λ_{H2} = 1.5 and λ_{Air} = 2.5.

The polarization curves displayed in Figure 6.10 were obtained after continuous operation for 5, 24 and 48 h at the same conditions as previously stated and the results from the testing is summarized in Table 6.6. Again, it can be observed that the performance of the **PBI-PPA**

membrane increases within the studied time period, likely due to the activation of the fuel cell. After 48 h of operation the OCV was 0.981 V. The relatively high OCV can be attributed to the mechanical strength of the membrane which provides a low membrane permeability, thus preventing significant gas cross-over between the electrodes. In the low current density region – up to roughly 0.2 A cm^{-2} – the voltage loss is mainly connected to the activation polarization which occurs due to the overpotential that is required to overcome the activation energy of the electrochemical reactions at each of the electrodes. The activation polarization is mainly dependent on the effectiveness of the catalysts and if the same catalyst attributes is used for two different MEAs the observed voltage is expected to be similar. At higher current densities, the voltage loss is primarily associated with the ohmic polarization which is caused by ohmic resistance from the cell components – of which the membrane resistance is the main contributor. When the current density is increased above roughly 0.8 A cm^{-2} the voltage loss increases due to mass transport limitations, however this region of the polarization curve was not studied in the present work.

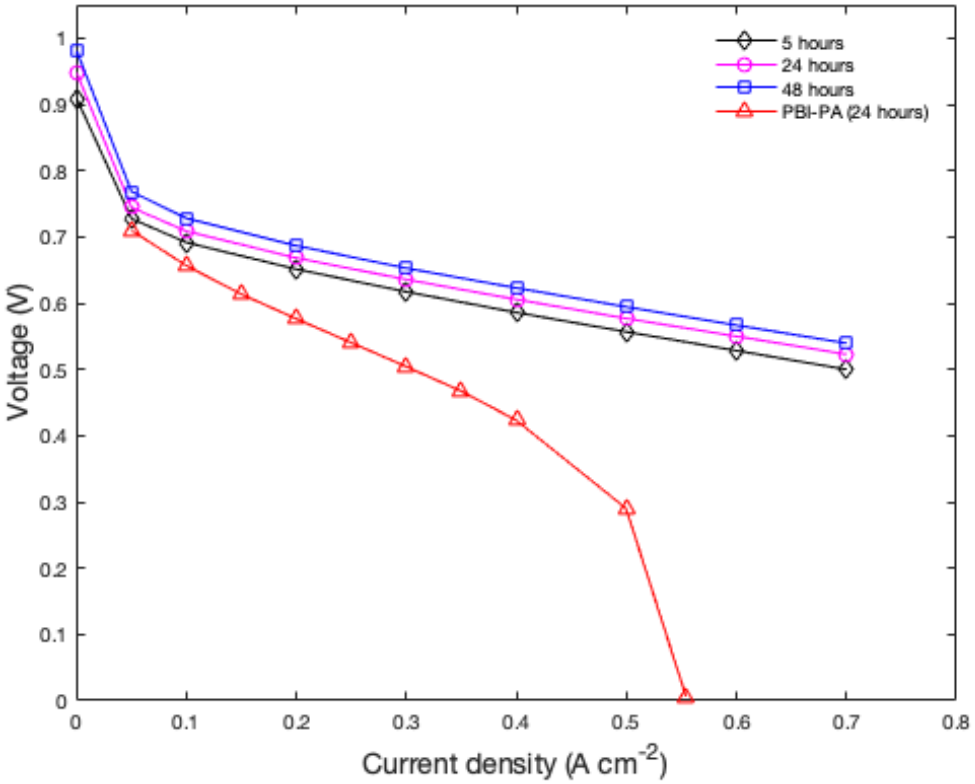

*Figure 6.10: Polarization curves from the MEA based on the **PBI-PPA** membrane after 5, 24 and 48 h of operation at a temperature of 160 ℃ and at a current density of 0.4 A cm^{-} . The polarization curve for the **PBI-PA** MEA after 24 h of operation under the same conditions is also displayed.*

As can be seen in Figure 6.11, the fuel cell performance of the **PBI-PPA** membrane is comparable to that from the Dapozol® membranes. The OCV after 48 h of operation was 0.981 V for the **PBI-PPA** MEA which can be compared to the corresponding values of 0.969 and 0.914 V for the high and low performance Dapozol® MEAs respectively. Commonly, the fuel

cell performance is estimated by a single point measurement at a specific current density. For an example, the **PBI-PPA** MEA provided a voltage of 0.687 V at 0.2 A cm^{-2} and the high and low performance Dapozol® MEAs produced voltages of 0.692 and 0.677 V respectively under the same conditions. In the linear region of the polarization curve it can be observed that the slope of the curve of the **PBI-PPA** MEA is in fact less than the reference MEAs which indicates a low ohmic polarization. This could possibly be explained by differences in the membrane thicknesses as well as the ADL since these parameters affect the proton conductivity [47]. Based on the results it can be presumed that the reprocessed PBI is sufficient to produce PEMs with similar fuel cell performance to what is seen using pristine PBI membranes.

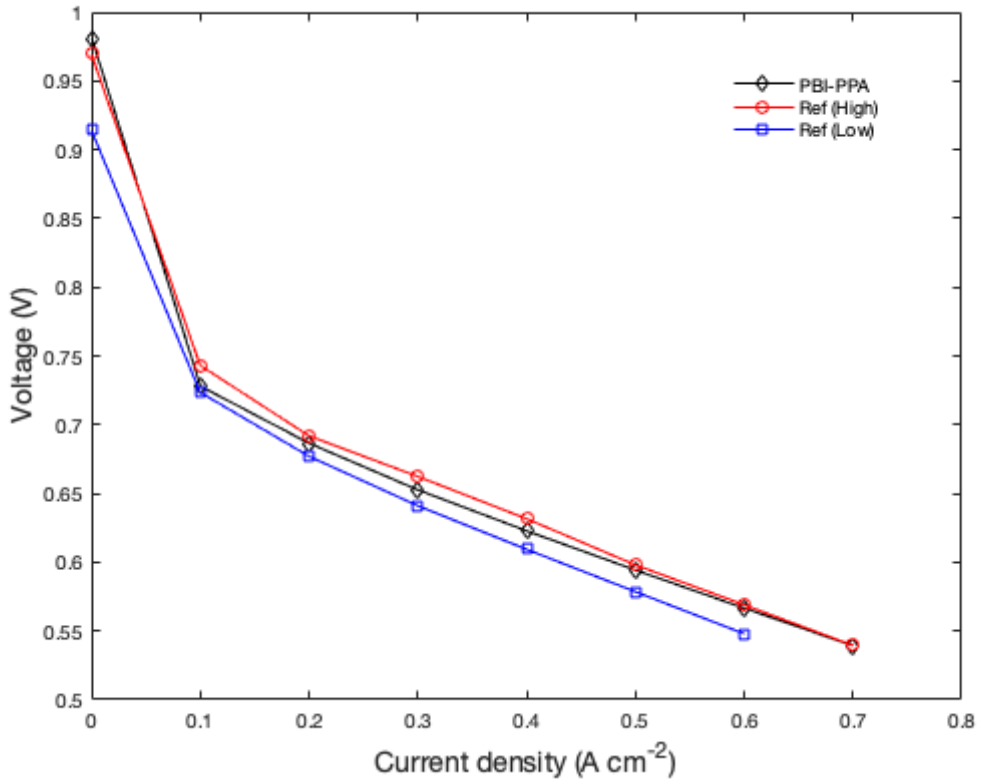

*Figure 6.11: Polarization curves after 48 hours of operation at 160 °C and a current density of 0.4 A cm^{-2} for the **PBI-PPA** MEA and the two reference MEAs.*

*Table 6.6: Summary of the cell performance at 160 °C of the **PBI-PPA** membrane. The membrane thickness in the undoped state and the obtained ADL after doping in 85 wt.% phosphoric acid is also reported in the table.*

		Cell voltage (V) after 48 h		
ADL	$Thickness_{dry}$ (µm)	OCV	0.2 A cm^{-2}	0.4 A cm^{-2}
10.2	37	0.981	0.687	0.624

7. Conclusion

The feasibility of recycling of phosphoric acid doped PBI membranes from the production line of Blue World Technologies has been investigated. Scrap membrane parts were successfully reprocessed by redissolution in both PPA and 85 wt.% PA at concentrations of 12 wt.% on the doped membrane basis. Slight deviations in the $\bar{M}_w$ between the reprocessed PBI and the reference material was observed, which may be due to hydrolysis of weak amide bonds present as structural defects in the pristine polymer. The reprocessing did not lead to any apparent change in the chemical structure of the PBI as determined by ^1H NMR and ATR FT-IR. After washing and drying, the obtained PBI powders were successfully dissolved in DMAc and membranes were casted by solvent evaporation from a 5 wt.% casting solution. Acid doping was performed by submerging the membranes in 85 wt.% PA which gave ADLs of roughly 10.5 and volumetric swellings that were in the range of 168-204%. The thermal stability of the undoped membranes was investigated by TGA and yielded a $T_{d,5\%}$ of 523-547 °C which is in agreement with what is expected for PBI. Tensile strengths at break of 19.2 and 19.3 MPa for doped membranes at room temperature were exhibited for the reprocessed samples which was slightly lower than for the reference material that had a corresponding value of 20.4 MPa. The proton conductivity under air without humidification was found to be between 0.064-0.070 S cm^{-1} at 160 °C for the reprocessed samples, which was also lower than the reference that had a corresponding value of 0.083 S cm^{-1}. The deviations that were observed in the tensile properties and the proton conductivity could reasonably be explained by inconsistencies in the membrane thickness and ADL. Finally, fuel cell testing indicated good performance of the reprocessed membrane that was comparable to what is attained when using pristine PBI membranes in commercial Dapozol® MEAs. For an example, the cell voltage after operation at 48 h at 160 °C and a constant current density of 0.2 A cm^{-2} was 0.687 V which can be compared to a high performance Dapozol® MEA that had a corresponding voltage of 0.692 V.

To summarize, the examined physicochemical properties of the PBI after reprocessing are largely unchanged in comparison to the pristine PBI. There was also no apparent difference in the properties depending on if PPA or PA was used as the solvent for the re-dissolution process. Fuel cell testing indicated good performance and short-term durability that was comparable to what is expected from pristine PBI membranes. Based on these observations, it is concluded that recycling of scrap PBI membranes can be a viable option in order to reduce material losses and the associated economic and environmental costs. Research should be continued to confirm the results of the study and also to evaluate other relevant properties, in addition to more extensive fuel cell testing.

8. Future work

The purpose of this section is to provide suggestions for future research on the topic.

- It is suggested that the work in the present study is repeated to confirm the results and findings in order to strengthen the viability of the attempted recycling method.
- Conduction of studies with the purpose of optimizing the recycling method with respect to the processing conditions. It is likely that the redissolution process could be improved, e.g. in terms of temperature and concentration, in order to minimize the energy and chemical consumption and maximize the process yield. Research on how to eliminate the need for the redissolution process to completely remove the doping acid from scrap membranes should be continued. The feasibility of up-scaling the process from lab-scale to a larger scale should also be taken into consideration.
- Further characterization and analysis of the properties of the reprocessed PBI membranes aside from the ones that has been examined in the present study should be performed to fully understand the practical implications and impact of the reprocessing on the PBI material. Other physicochemical properties that could be investigated include the oxidative stability and gas permeability which are properties that are influential towards the longevity and performance of the PBI membrane and would therefore be of interest to characterize.
- More extensive testing of the fuel cell performance. The reprocessed PBI membrane in the present work was only evaluated by testing under a relatively short time period. The durability of the fuel cell is of critical importance with requirements on consistent performance during operation for thousands of hours depending on the application. Furthermore, the fuel cell testing was only carried out at one operation temperature at a relatively low current density. It is suggested that the fuel cell performance is further investigated with a focus on evaluating the long-term performance as well as the operation under more harsh conditions in terms of issues related to PA wash out, evaporation and catalyst dissolution.
- Investigation of the repeated recycling of scrap PBI. In the present work, the attempted reprocessing method was only applied in one cycle. It is known that repeated reprocessing of polymer materials may lead to degradation of the molecular weight which may lead to significant loss of properties after a certain amount of cycles. Therefore, it would be of interest to examine the effects of repeated recycling of scrap PBI to investigate how it influences the properties of the polymer.
- Investigating the blending of pristine and recycled PBI could also be of interest if it is found that the reprocessing deteriorates the quality of the polymer, e.g. by reducing the molecular weight outside of the range that is required for membrane production.

9. References

[1] R. He, Q. Li, A. Bach, J. O. Jensen, and N. J. Bjerrum, "Physicochemical properties of phosphoric acid doped polybenzimidazole membranes for fuel cells," *J Memb Sci*, vol. 277, no. 1–2, pp. 38–45, Jun. 2006, doi: 10.1016/j.memsci.2005.10.005.

[2] A. Chandan *et al.*, "High temperature (HT) polymer electrolyte membrane fuel cells (PEMFC)-A review," *Journal of Power Sources*, vol. 231. pp. 264–278, 2013. doi: 10.1016/j.jpowsour.2012.11.126.

[3] Q. Li, R. He, J. O. Jensen, and N. J. Bjerrum, "PBI-based polymer membranes for high temperature fuel cells - Preparation, characterization and fuel cell demonstration," *Fuel Cells*, vol. 4, no. 3. pp. 147–159, Aug. 2004. doi: 10.1002/fuce.200400020.

[4] J. S. Wainright, J. T. Wang, D. Weng, R. F. Savinell, and M. Litt, "Acid-doped polybenzimidazoles - A new polymer electrolye," *J Electrochem Soc*, vol. 142, no. 7, pp. L121–L123, Jul. 1995, doi: 10.1149/1.2044337.

[5] Blue World Technologies, "About Us." 2022. [Online] https://www.blue.world/about-us/. [Accessed: 2023-04-12]

[6] K. S. Dhathathreyan and N. Rajalakshmi, "3. Polymer Electrolyte Membrane Fuel Cell." *Recent Trends in Fuel Cell Science and Technology.* pp. 40-115. New Delhi, India: Springer, 2007.

[7] J. Zhang *et al.*, "High temperature PEM fuel cells," *Journal of Power Sources*, vol. 160, no. 2 SPEC. ISS. Elsevier, pp. 872–891, Oct. 06, 2006. doi: 10.1016/j.jpowsour.2006.05.034.

[8] K. Hamad, M. Kaseem, and F. Deri, "Recycling of waste from polymer materials: An overview of the recent works," *Polymer Degradation and Stability*, vol. 98, no. 12. pp. 2801–2812, Dec. 2013. doi: 10.1016/j.polymdegradstab.2013.09.025.

[9] L. Delva *et al.*, "An Introductory Review: Mechanical recycling of polymers for dummies." Ghent University, Belgium. 2018.

[10] SITRA, "The Circular Economy a Powerful Force for Climate Mitigation Transformative innovation for prosperous and low-carbon industry", Stockholm, 2018.

[11] M. L. Henriksen, C. B. Karlsen, P. Klarskov, and M. Hinge, "Plastic classification via in-line hyperspectral camera analysis and unsupervised machine learning," *Vib Spectrosc*, vol. 118, Jan. 2022, doi: 10.1016/j.vibspec.2021.103329.

[12] "Plastics: Material-Specific data," *United States Environemntal Protection Agency*, Apr. 23, 2023.

[13] D. Aili, J. Yang, K. Jankova, D. Henkensmeier, and Q. Li, "From polybenzimidazoles to polybenzimidazoliums and polybenzimidazolides," *Journal of Materials Chemistry A*, vol. 8, no. 26. Royal Society of Chemistry, pp. 12854–12886, Jul. 14, 2020. doi: 10.1039/d0ta01788d.

[14] R. B. Sandor, "PBI (Polybenzimidazole): Synthesis, Properties and Applications." in *Materials Science: High Performance Polymers*, vol. 2, no. 1, Feb. 1, 1990. doi: 10.1177/152483999000200103

[15] H. Vogel and C. S. Marvel, “Polybenzimidazoles, new thermally stable polymers,” *Journal of Polymer Science*, vol. 50, no. 154, pp. 511–539, Apr. 1961, doi: 10.1002/pol.1961.1205015419.

[16] Y. Iwakura, Y. Imai, and K. Uno, “Polyphenylenebenzimidazoles” *Journal of Polymer Science Part A-General Papers* vol. 2, no. 6PA, pp. 2605-, 1964, doi: 10.1002/pol.1964.100020611.

[17] E. W. Neuse, “Aromatic Polybenzimidazoles - Syntheses properties and applications,” *Advances in Polymer Science*, vol. 47, pp. 1–42, 1982.

[18] J. M. G. Cowie and V. Arrighi, *Polymers: Chemistry and Physics of Modern Materials*, 3rd ed. Boca Raton, FL: CRC Press, 2007.

[19] E. Quartarone and P. Mustarelli, “Polymer fuel cells based on polybenzimidazole/H3PO4,” *Energy Environ Sci*, vol. 5, no. 4, pp. 6436–6444, Apr. 2012, doi: 10.1039/c2ee03055a.

[20] M. Nuchter, B. Ondruschka, W. Bonrath, and A. Gum, “Microwave assisted synthesis - a critical technology overview,” *Green Chemistry*, vol. 6, no. 3, pp. 128–141, 2004, doi: 10.1039/b310502d.

[21] A. Buckley, D. Stuetz, and G. Serad, “Polybenzimidazoles,” in *Encyclopedia of Polymer Science and ngineering*, II.New York: Wiley, 1987, pp. 572–601.

[22] D. Aili, L. N. Cleemann, Q. Li, J. O. Jensen, E. Christensen, and N. J. Bjerrum, “Thermal curing of PBI membranes for high temperature PEM fuel cells,” *J Mater Chem*, vol. 22, no. 12, pp. 5444–5453, Mar. 2012, doi: 10.1039/c2jm14774b.

[23] B. G. Dawkins, F. Qin, M. Gruender, and G. S. Copeland, “Polybenzimidazole (PBI) high temperature polymers and blends,” in *High Temperature Polymer Blends*, Elsevier Inc., 2014, pp. 174–212. doi: 10.1533/9780857099013.174.

[24] J. S. Yang *et al.*, “High molecular weight polybenzimidazole membranes for high temperature PEMFC,” *Fuel Cells*, vol. 14, no. 1, pp. 7–15, Feb. 2014, doi: 10.1002/fuce.201300070.

[25] Q. F. Li *et al.*, “Properties, degradation and high temperature fuel cell test of different types of PBI and PBI blend membranes,” *J Memb Sci*, vol. 347, no. 1–2, pp. 260–270, Feb. 2010, doi: 10.1016/j.memsci.2009.10.032.

[26] A. Sannigrahi, D. Arunbabu, R. Murali Sankar, and T. Jana, “Aggregation behavior of polybenzimidazole in aprotic polar,” *Macromolecules*, vol. 40, no. 8, pp. 2844–2851, Apr. 2007, doi: 10.1021/ma070049q.

[27] E. Feketel, Z. Peredy’, E. Foldes’, F. E. Karasz, and B. Pukanszky, “Effect of specific interactions on film casting of high temperature polymers,” in *Polymer Bulletin*, vol 39, pp. 93-99, 1997.

[28] D. Aili, J. O. Jensen, and Q. Li, “Polybenzimidazole membranes by Post Acid Doping,” in *High Temperature Polymer Electrolyte Membrane Fuel Cells: Approaches, status and perspectives*, D. Aili, Q. Li, H. A. Hjuler, and J. O. Jensen, Eds., Springer, 2016, pp. 195–215.

[29] B. Wang, Y. Tang, Z. Wen, and H. Wang, “Dissolution and regeneration of polybenzimidazoles using ionic liquids,” *Eur Polym J*, vol. 45, no. 10, pp. 2962–2965, Oct. 2009, doi: 10.1016/j.eurpolymj.2009.07.001.

[30] Q. F. Li *et al.*, "Properties, degradation and high temperature fuel cell test of different types of PBI and PBI blend membranes," *J Memb Sci*, vol. 347, no. 1–2, pp. 260–270, Feb. 2010, doi: 10.1016/j.memsci.2009.10.032.

[31] G. Qian and B. C. Benicewicz, "Synthesis and characterization of high molecular weight hexafluoroisopropylidene-containing polybenzimidazole for high-temperature polymer electrolyte membrane fuel cells," *J Polym Sci A Polym Chem*, vol. 47, no. 16, pp. 4064–4073, Aug. 2009, doi: 10.1002/pola.23467.

[32] D. Aili *et al.*, "Polybenzimidazole-Based High-Temperature Polymer Electrolyte Membrane Fuel Cells: New Insights and Recent Progress," *Electrochemical Energy Reviews*, vol. 3, no. 4. Springer Science and Business Media B.V., pp. 793–845, Dec. 01, 2020. doi: 10.1007/s41918-020-00080-5.

[33] R. Bouchet and E. Siebert, "Proton conduction in acid doped polybenzimidazole," in *Solid State Ionics,* vol.118, no. 3-4, pp. 287-299. Mar. 1999. doi: 10.1016/s0167273898004664-4.

[34] B. Z. Xing and O. Savadogo, "The effect of acid doping on the conductivity of polybenzimidazole (PBI)," *Journal of New Materials for Electrochemical Systems,"* vol. 2, no. 2, pp. 95–101, Apr. 1999.

[35] Q. Li, R. He, R. W. Berg, H. A. Hjuler, and N. J. Bjerrum, "Water uptake and acid doping of polybenzimidazoles as electrolyte membranes for fuel cells," *Solid State Ion*, vol. 168, no. 1–2, pp. 177–185, Mar. 2004, doi: 10.1016/j.ssi.2004.02.013.

[36] D. Aili *et al.*, "Phosphoric Acid Dynamics in High Temperature Polymer Electrolyte Membranes," *J Electrochem Soc*, vol. 167, no. 13, p. 134507, Sep. 2020, doi: 10.1149/1945-7111/abb70c.

[37] C. B. Shogbon, J. L. Brousseau, H. Zhang, B. C. Benicewicz, and Y. A. Akpalu, "Determination of the molecular parameters and studies of the chain conformation of polybenzimidazole in DMAc/LiCl," *Macromolecules*, vol. 39, no. 26, pp. 9409–9418, Dec. 2006, doi: 10.1021/ma0609836.

[38] T. Steenberg, H. A. Hjuler, C. Terkelsen, M. T. R. Sánchez, L. N. Cleemann, and F. C. Krebs, "Roll-to-roll coated PBI membranes for high temperature PEM fuel cells," *Energy Environ Sci*, vol. 5, no. 3, pp. 6076–6080, Mar. 2012, doi: 10.1039/c2ee02936g.

[39] L. Xiao *et al.*, "High-Temperature Polybenzimidazole Fuel Cell Membranes via a Sol-Gel Process," 2005, doi: 10.1021/cm050831.

[40] M. Litt, R. Ameri, Y. Wang, R. Savinell, and J. Wainwright, "Polybenzimidazoles/phosphoric acid solid polymer electrolytes: Mechanical and electrical properties," in *Materials Research Society Symposium Proceedings*, G. Nazi, C. Julien, and A. Rougier, Eds., 1999, pp. 313–323.

[41] D. Aili and D. Henkensmeier, "Techniques for PBI Membrane Characterization," in *High Temperature Polymer Electrolyte Membrane Fuel Cells*, D. Aili, Q. Li, H. A. Hjuler, and J. O. Jensen, Eds., 2016, pp. 127–150.

[42] Y. Yuan, F. Johnson, and I. Cabasso, "Polybenzimidazole (FBI) molecular weight and Mark-Houwink equation," *J Appl Polym Sci*, vol. 112, no. 6, pp. 3436–3441, Jun. 2009, doi: 10.1002/app.29817.

[43] C. E. Hughes *et al.*, “Probing structure and dynamics in poly[2,2′-(m-phenylene)-5,5′-bibenzimidazole] fuel cells with magic-angle spinning NMR,” *Journal of Physical Chemistry B*, vol. 108, no. 36, pp. 13626–13631, Sep. 2004, doi: 10.1021/jp047607c.

[44] J. Yang, R. He, Q. Che, X. Gao, and L. Shi, “A copolymer of poly[2,2′-(m-phenylene)-5,5′- bibenzimidazole] and poly(2,5-benzimidazole) for high-temperature proton-conducting membranes,” *Polym Int*, vol. 59, no. 12, pp. 1695–1700, Dec. 2010, doi: 10.1002/pi.2906.

[45] P. Musto, F. E. Karaszt, and W. J. Macknight, “Fourier transform infra-red spectroscopy on the thermo-oxidative degradation of polybenzimidazole and of a polybenzimidazole / polyetherimide blend,” Department of Polymer Science and Engineering, University of Massachusetts, USA. 1993.

[46] G. Guerra, S. Choe, D. J. Williams, F. E. Karasz, and W. J. Macknight, “Fourier Transform Infrared Spectroscopy of Some Miscible Polybenzimidazole/Polyimide Blends,” 1988. [Online]. Available: https://pubs.acs.org/sharingguidelines

[47] Y. Chen *et al.*, “Feasibility of using thin polybenzimidazole electrolytes in high-temperature proton exchange membrane fuel cells,” *Int J Hydrogen Energy*, vol. 47, no. 66, pp. 28615–28625, Aug. 2022, doi: 10.1016/j.ijhydene.2022.06.156.

[48] F. Ameli, S. Moghadam, and S. Shahmarvand, “Polymer flooding,” in *Chemical Methods*, Elsevier, 2021, pp. 33–94. doi: 10.1016/B978-0-12-821931-7.00003-1.

[49] J. Lobato, P. Cañizares, M. A. Rodrigo, J. J. Linares, and G. Manjavacas, “Synthesis and characterisation of poly[2,2-(m-phenylene)-5,5-bibenzimidazole] as polymer electrolyte membrane for high temperature PEMFCs,” *J Memb Sci*, vol. 280, no. 1–2, pp. 351–362, Sep. 2006, doi: 10.1016/j.memsci.2006.01.049.

[50] D. Aili *et al.*, “Polybenzimidazole and sulfonated polyhedral oligosilsesquioxane composite membranes for high temperature polymer electrolyte membrane fuel cells,” *Electrochim Acta*, vol. 140, pp. 182–190, Sep. 2014, doi: 10.1016/j.electacta.2014.03.047.

[51] Y.-L. Ma, J. S. Wainright, M. H. Litt, and R. F. Savinell, “Conductivity of PBI Membranes for High-Temperature Polymer Electrolyte Fuel Cells,” *J Electrochem Soc*, vol. 151, no. 1, p. A8, 2004, doi: 10.1149/1.1630037.

[52] S. Thomas, S. S. Araya, J. R. Vang, and S. K. Kær, “Investigating different break-in procedures for reformed methanol high temperature proton exchange membrane fuel cells,” *Int J Hydrogen Energy*, vol. 43, no. 31, pp. 14691–14700, Aug. 2018, doi: 10.1016/j.ijhydene.2018.05.166.

10. Appendix

10.1 Appendix A: Stress-strain curves

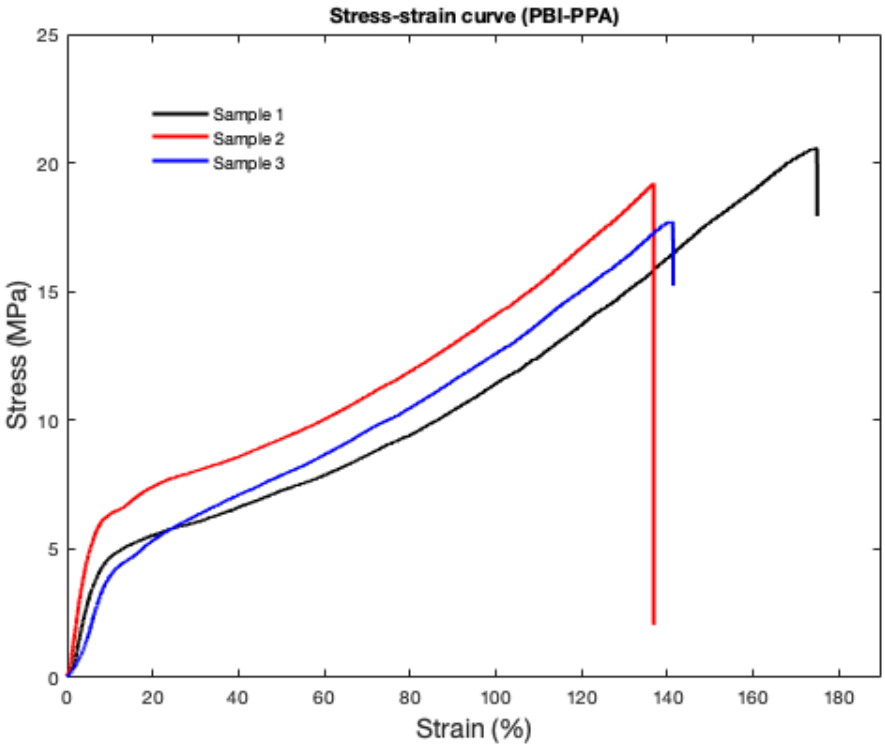

Figure 10.1: Stress-strain curve at room temperature displaying three different samples from ***PBI-PPA.***

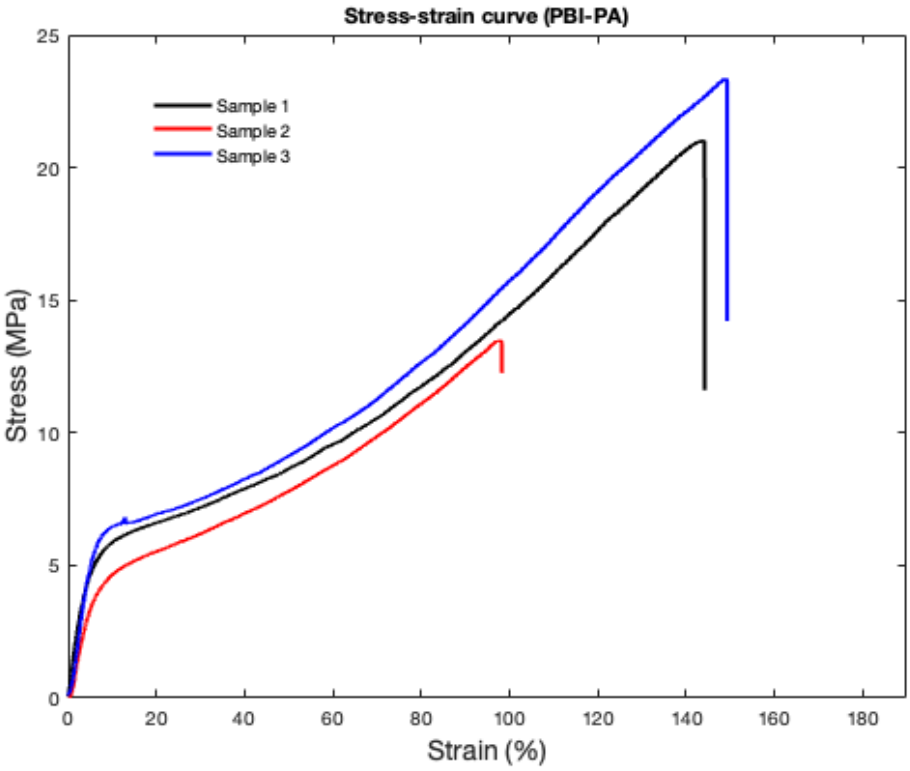

Figure 10.2: Stress-strain curve at room temperature displaying three different samples from ***PBI-PA.***

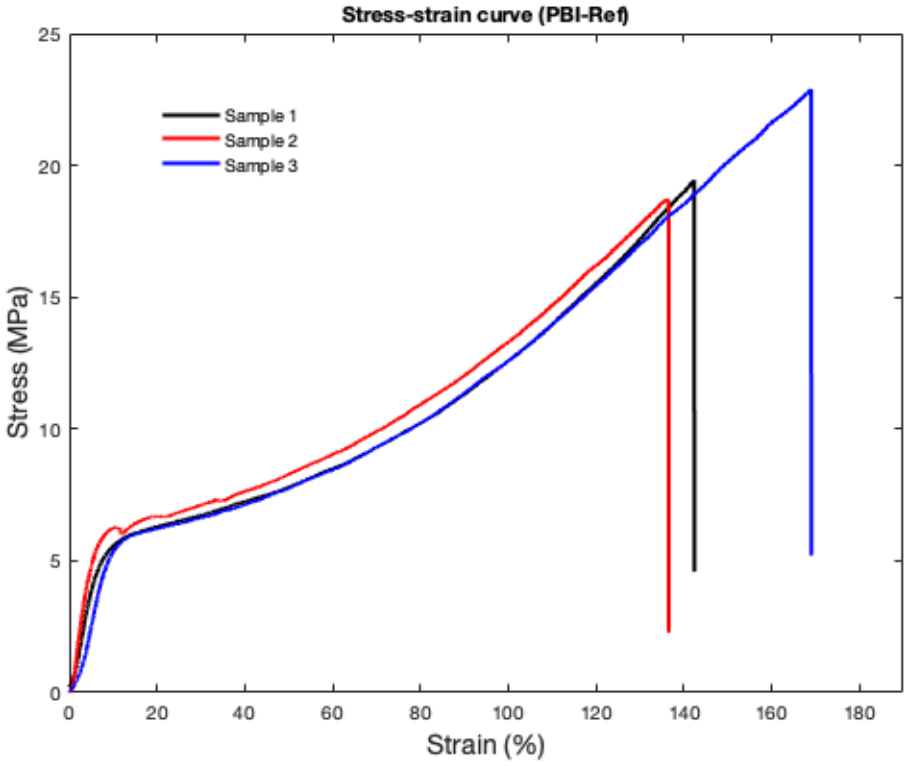

Figure 10.3: Stress-strain curve at room temperature displaying three different samples from ***PBI-Ref.***